Cell Reports
Medicine

Article

Inhibiting 3βHSD1 to eliminate the oncogenic effects of progesterone in prostate cancer

Graphical abstract

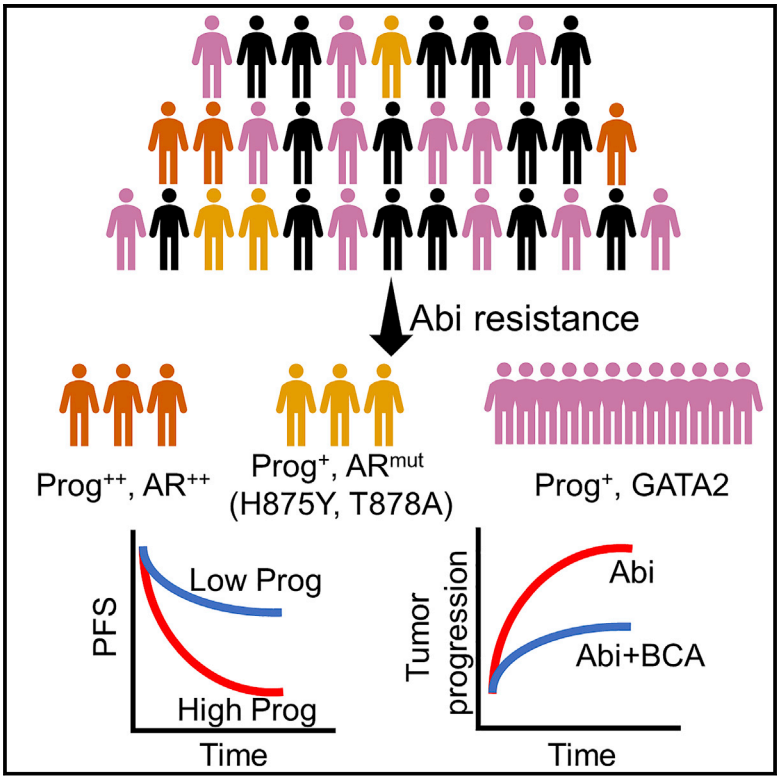

Highlights

- High doses of progesterone activate canonical and non-canonical AR signaling
- Progesterone of physiological levels exerts its chronic oncogenic effect via GATA2
- Targeting 3βHSD1 to suppress progesterone synthesis blocks its oncogenic effects
- Serum progesterone might be a predictive biomarker for abiraterone response

Authors

Zemin Hou, Shengsong Huang, Zejie Mei, ..., Huiru Tang, Denglong Wu, Zhenfei Li

Correspondence

zhenfei.li@sibcb.ac.cn (Z.L.), Wudenglong2009@tongji.edu.cn (D.W.), huiru_tang@fudan.edu.cn (H.T.)

In brief

Hou et al. identify that progesterone of different levels exerted oncogenic effects in prostate cancer cells via different mechanisms. Strategies targeting 3βHSD1 inhibit the transient and chronic oncogenic effects of progesterone. Serum progesterone is also found to be a potential predictive biomarker for abiraterone response.

Hou et al., 2022, Cell Reports Medicine 3, 100561
March 15, 2022
https://doi.org/10.1016/j.xcrm.2022.100561

CellPress

Cell Reports Medicine

CellPress
OPEN ACCESS

Article

Inhibiting 3βHSD1 to eliminate the oncogenic effects of progesterone in prostate cancer

Zemin Hou,[1,9] Shengsong Huang,[2,9] Zejie Mei,[1,9] Longlong Chen,[3,9] Jiacheng Guo,[4] Yuanyuan Gao,[1] Qian Zhuang,[1] Xuebin Zhang,[1] Qilong Tan,[1] Tao Yang,[2] Ying Liu,[2] Yongnan Chi,[2] Lifengrong Qi,[5] Ting Jiang,[6] Xuefeng Shao,[6] Yan Wu,[7] Xiaojun Xu,[5] Jun Qin,[4] Ruobing Ren,[7,8] Huiru Tang,[3,*] Denglong Wu,[2,*] and Zhenfei Li[1,2,10,*]

[1]State Key Laboratory of Cell Biology, CAS Center for Excellence in Molecular Cell Science, Shanghai Institute of Biochemistry and Cell Biology, Chinese Academy of Sciences, University of Chinese Academy of Sciences, 320 Yueyang Road, Shanghai 200031, China
[2]Department of Urology, Tongji Hospital, School of Medicine, Tongji University, Shanghai 200065, China
[3]State Key Laboratory of Genetic Engineering, School of Life Sciences, Human Phenome Institute, Metabonomics and Systems Biology Laboratory at Shanghai International Centre for Molecular Phenomics, Zhongshan Hospital, Fudan University, Shanghai 200438, China
[4]CAS Key Laboratory of Tissue Microenvironment and Tumor, Shanghai Institute of Nutrition and Health, University of Chinese Academy of Sciences, Chinese Academy of Sciences, 320 Yueyang Road, Shanghai 200031, China
[5]State Key Laboratory of Natural Medicines, China Pharmaceutical University, Nanjing 210009, Jiangsu, China
[6]Department of Urology, First People's Hospital of Taicang, Taicang, Jiangsu 215400, China
[7]Shanghai Key Laboratory of Metabolic Remodeling and Health, Institute of Metabolism and Integrative Biology, Fudan University, Shanghai, China
[8]Kobilka Institute of Innovative Drug Discovery, School of Life and Health Sciences, the Chinese University of Hong Kong, Shenzhen, Guangdong 518172, China
[9]These authors contributed equally
[10]Lead contact
*Correspondence: zhenfei.li@sibcb.ac.cn (Z.L.), Wudenglong2009@tongji.edu.cn (D.W.), huiru_tang@fudan.edu.cn (H.T.)
https://doi.org/10.1016/j.xcrm.2022.100561

SUMMARY

Prostate cancer continuously progresses following deprivation of circulating androgens originating from the testis and adrenal glands, indicating the existence of oncometabolites beyond androgens. In this study, mass-spectrometry-based screening of clinical specimens and a retrospective analysis on the clinical data of prostate cancer patients indicate the potential oncogenic effects of progesterone in patients. High doses of progesterone activate canonical and non-canonical androgen receptor (AR) target genes. Physiological levels of progesterone facilitate cell proliferation via GATA2. Inhibitors of 3β-hydroxysteroid dehydrogenase 1 (3βHSD1) has been discovered and shown to suppress the generation of progesterone, eliminating its transient and accumulating oncogenic effects. An increase in progesterone is associated with poor clinical outcomes in patients and may be used as a predictive biomarker. Overall, we demonstrate that progesterone acts as an oncogenic hormone in prostate cancer, and strategies to eliminate its oncogenic effects may benefit prostate cancer patients.

INTRODUCTION

The progression of prostate cancer is reliant on androgens.[1,2] Testosterone synthesized from the testis is a major oncogenic androgen in prostate cancer.[3] Androgen deprivation therapy (ADT) significantly reduces the levels of circulating testosterone to castration levels.[4] Consequently, dehydroepiandrosterone (DHEA), the adrenal androgen precursor, is utilized by prostate cancer cells for the synthesis of dihydrotestosterone (DHT).[2] Abiraterone inhibits the steroidogenic enzyme cytochrome P450 17A1 (CYP17A1) to suppress the generation of DHEA.[5] The combination of ADT and abiraterone leads to an androgen-deficient environment in patients. However, disease progression is inevitable, and prostate cancer cells might utilize alternative oncometabolites to fuel proliferation.

Multiple mechanisms have been proposed to explain this inexorable disease progression, including androgen-independent AR-v7 and neuroendocrine prostate cancer cells.[6–9] Accumulating evidence also supports the existence of other oncometabolites in prostate cancer. AR mutations and the glucocorticoid receptor (GR) facilitate the affinity of prostate cancer cells for steroids beyond androgens.[10–12] The AR T878A mutant found in LNCaP cells has expanded substrates, and the AR L702H and T878A mutant found in MDA PCa2b cells responds to corticosteroids.[11,13] Steroids share the common cyclopentanophenanthrene four-ring structure with androgens, and might exert an oncogenic effect on prostate cancer, dependent or independent on AR.[10,11,14] However, these effects are overshadowed by the potent function of androgens, and patients receiving a combination therapy of ADT and abiraterone could provide a unique model to discover novel oncometabolites. Improvements in mass spectrometry (MS) also increase the possibility of identifying novel oncometabolites, even with limited patient specimens.

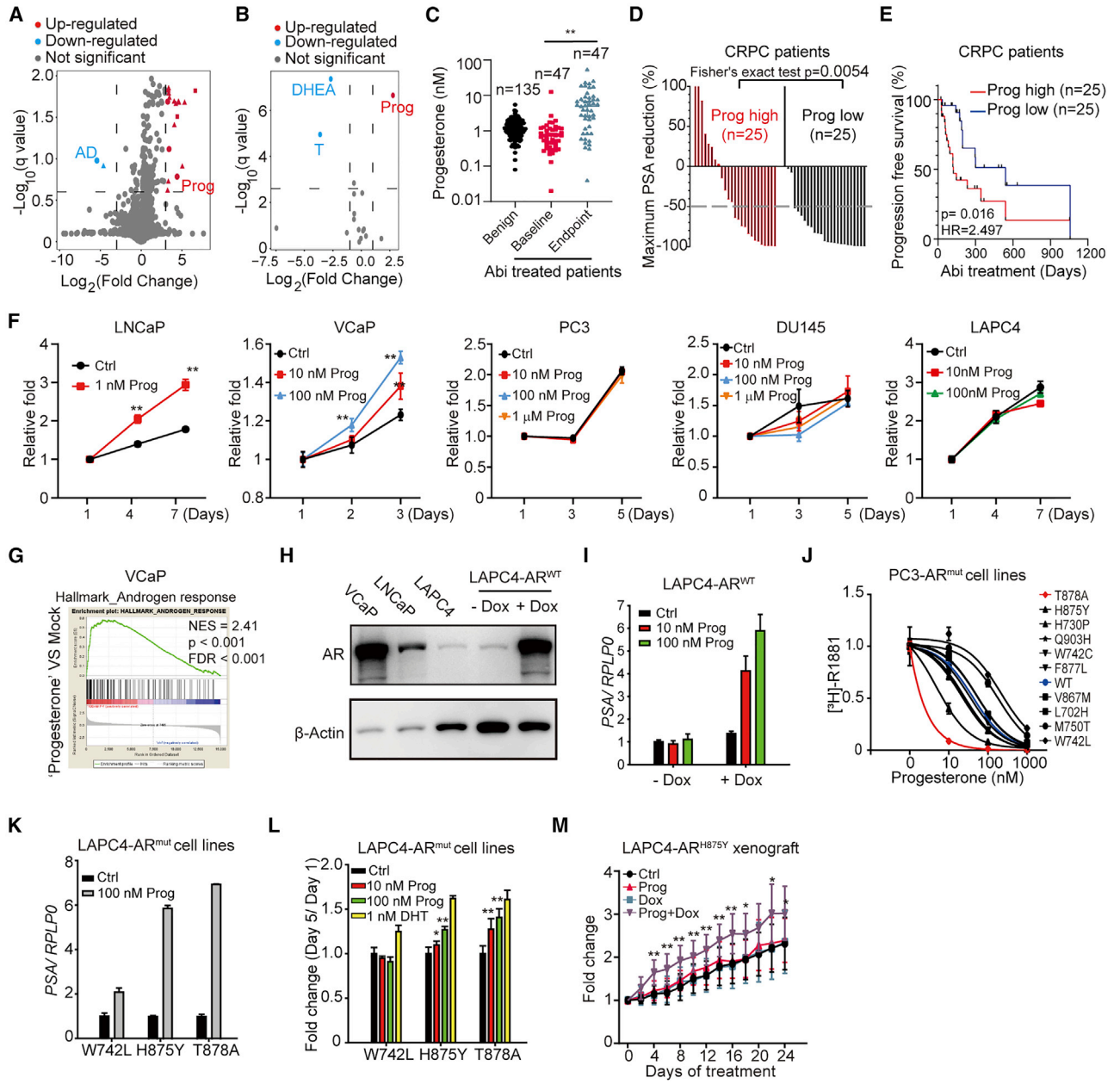

Figure 1. The transient oncogenic effects of progesterone via the AR

(A) Alterations of plasma metabolites in prostate cancer patients after abiraterone treatment. Paired plasma samples were collected from 10 patients before and after abiraterone treatment for mass spectrometry (MS) analysis. Circle, metabolites with determined structure; triangle, metabolites with undetermined structure; square, abiraterone metabolites; Prog, progesterone; AD, androstenedione. Each data point represents the mean alteration of one metabolite in these 10 paired samples.

(B) Alterations in endocrine-hormone-related laboratory indices in patients after abiraterone treatment. Details on laboratory indices are shown in Figure S1C.

(C) Plasma progesterone levels in benign patients (n = 135) and prostate cancer patients receiving abiraterone treatment (n = 47). Paired Student's t test.

(D) CRPC patients with high levels of plasma progesterone had a less potent PSA reduction after abiraterone treatment. Fisher's exact test.

(E) CRPC patients with high levels of plasma progesterone had a shorter abiraterone treatment duration. Disease progression was determined by PSA according to PCWG2 guidelines. Log rank test. Patients were grouped based on their plasma progesterone concentrations at the endpoint (D and E).

(F) Effects of progesterone on cell proliferation. Different prostate cancer cell lines were used for the cell proliferation assay.

(G) Gene set enrichment analysis (GSEA) on androgen response of MSigDB hallmark set in progesterone-treated VCaP cells. Progesterone (100 nM) was used to treat VCaP cells before RNA sequencing (RNA-seq) assay. Biological replicate, n = 3.

(H) AR abundance in different cell lines. LAPC4-AR^{WT}, LAPC4 cells expressing the doxycycline (Dox, 1 μg/mL) induced wild-type AR.

(I) Effects of progesterone in the LAPC4-AR^{WT} cells on AR target gene expression.

(legend continued on next page)

In this study, we performed an MS-based metabolite screening of plasma samples from patients receiving ADT and abiraterone treatment. Clinical information was evaluated to identify novel oncometabolites. We also investigated the functional mechanisms and potential clinical applications of the identified oncometabolites.

RESULTS

Screening of potential oncometabolites

To identify novel oncometabolites driving disease progression, paired plasma samples were collected from 10 patients, before and after abiraterone treatment, and screened via ultrahigh-performance chromatography (UHPLC)-MS (Table S1). Untargeted metabolomics analysis (5,531 metabolites detected) and targeted simultaneous quantification of lipidomic and sterol metabolites (1,094 metabolites detected) were performed. Among the total 6,625 metabolites, progesterone was one of the most increased metabolites and androstenedione (AD) had the greatest decrease, following abiraterone treatment (Figure 1A). Further analysis of the alterations in sterol levels in patient samples, determined by a UHPLC-tandem MS (MS/MS) system in multiple-reaction monitoring mode with a quantitative sensitivity well above previous reports, revealed that most of the metabolites involved in progesterone metabolism changed significantly after abiraterone treatment (Figures S1A and S1B).[15,16]

Clinical data from patients (N = 73) receiving ADT and abiraterone treatment between August 2016 and April 2020 at the Shanghai Tongji Hospital, including endocrine-hormone-related laboratory indices and treatment response, were also evaluated to identify potential oncogenic hormones (Table S2). Baseline data were from the beginning of abiraterone treatment and the endpoint of observation was either the date of disease progression or April of 2020. Among the 17 hormone-related laboratory indices, progesterone was the most significantly increased metabolite, following abiraterone treatment (Figures 1B, 1C, and S1C). The increase in plasma progesterone was observed in both castration-resistant prostate cancer (CRPC) patients and hormone-sensitive prostate cancer (HSPC) patients (Figure S1D). Patients with a higher plasma progesterone concentration at the endpoint showed poor clinical outcomes, including a less potent prostate-specific antigen (PSA) reduction and shorter treatment duration (Figures S1E and S1F). To exclude a potential disturbance in ADT, the correlation between plasma progesterone concentration and treatment response was further analyzed in CRPC patients only (Table S3). CRPC patients with higher plasma concentrations of progesterone at the endpoint also exhibited a less potent PSA reduction and earlier disease progression (Figures 1D and 1E). Together, these data corroborate previous findings that progesterone is important for prostate cancer and indicate that progesterone is a potential oncogenic hormone in prostate cancer.[17,18]

Canonical AR signaling regulated by progesterone

To investigate the oncogenic effects of progesterone, different prostate cancer cell lines were treated with progesterone for the cell proliferation assay. Phenol red-free medium plus 5% charcoal-stripped serum (CSS) was used for cell proliferation assay and progesterone promoted cell growth in AR-positive cell lines (LNCaP and VCaP) but not in AR-negative cell lines (PC3 and DU145) (Figure 1F). In LNCaP and VCaP cells, progesterone activated the expression of AR target genes, which were inhibited by the AR antagonist enzalutamide (Figures S2A and S2B).[19,20] Transcriptome analysis of VCaP cells confirmed the activation of AR signaling after progesterone treatment (Figure 1G). Progesterone receptor (PR) was detectable in VCaP cells but not in other prostate cancer cell lines (Figure S2C). Knockdown of PR in VCaP cells resulted in limited effects on cell proliferation in VCaP cells (Figures S2D and S2E). These results demonstrate that the progesterone-induced cell proliferation in LNCaP and VCaP cells is dependent on AR but not PR. Due to the limited abundance of AR in LAPC4 cells, progesterone had no effect on the proliferation of LAPC4 cells (Figure 1F). A stable cell line was established in LAPC4 cells with doxycycline (Dox)-induced AR expression (LAPC4-AR^{WT}) (Figure 1H). The addition of Dox induced AR but not PR expression in LAPC4-AR^{WT} cells (Figure S2F). Progesterone activated AR signaling in LAPC4-AR^{WT} cells only when Dox was added (Figure 1I). Together, these data consistently demonstrate that progesterone exerts its oncogenic effects via the AR.[17,18]

Progesterone also increased AR abundance and facilitated AR nuclear accumulation (Figures S2G–S2I). These effects were more obvious in LNCaP cells, indicating that the AR genotype is essential for the function of progesterone. Plasmids expressing different AR mutants were used to generate stable cell lines in PC3 cells for competition assays. Progesterone showed a high affinity for AR^{T878A} (with broadened ligands) and AR^{H875Y} (resistant to bicalutamide; sensitive to darolutamide),[21] but a low affinity for AR^{W742L} (activated by bicalutamide)[22] and AR^{M750T} (Figure 1J). A PSA-luciferase reporter was then used to evaluate the oncogenic effects of progesterone. Progesterone significantly activated AR^{T878A} and AR^{H875Y} but not AR^{W742L} and AR^{M750T} in the reporter system (Figures S2J and S2K). Thus, progesterone activated AR signaling and promoted cell proliferation in LAPC4 cell lines stably expressing Dox-induced AR^{T878A} or

(J) Affinity of progesterone to different AR mutants. The PC3 stable cell lines expressing wild-type AR or different AR mutants were used for competition assays. Progesterone was used to compete 1 nM [^{3}H]-R1881 to bind to AR. Biological replicate, n = 3.

(K) Progesterone-activated AR^{H875Y} and AR^{T878A}-mediated AR signaling. LAPC4 cells consistently expressing AR^{H875Y} or AR^{T878A} were treated with 100 nM progesterone.

(L) Progesterone promoted AR^{H875Y}- and AR^{T878A}-mediated cell proliferation. LAPC4 cells consistently expressing AR^{H875Y} or AR^{T878A} were treated with progesterone and DHT for cell proliferation assays.

(M) Oncogenic effect of progesterone on the LAPC4-AR^{H875Y} xenografts. LAPC4 cells expressing inducible AR^{H875Y} were used for xenograft assays. Progesterone was administered via 15-mg sustained-release pellets. Dox, 2 mg/mL in water. Each group had 10 mice. Results are represented as means ± SD. Experiments were performed at least three times independently. $^{**}p < 0.01$; $^{*}p < 0.05$ (see also Figures S1, S2A–S2K; Tables S1–S3).

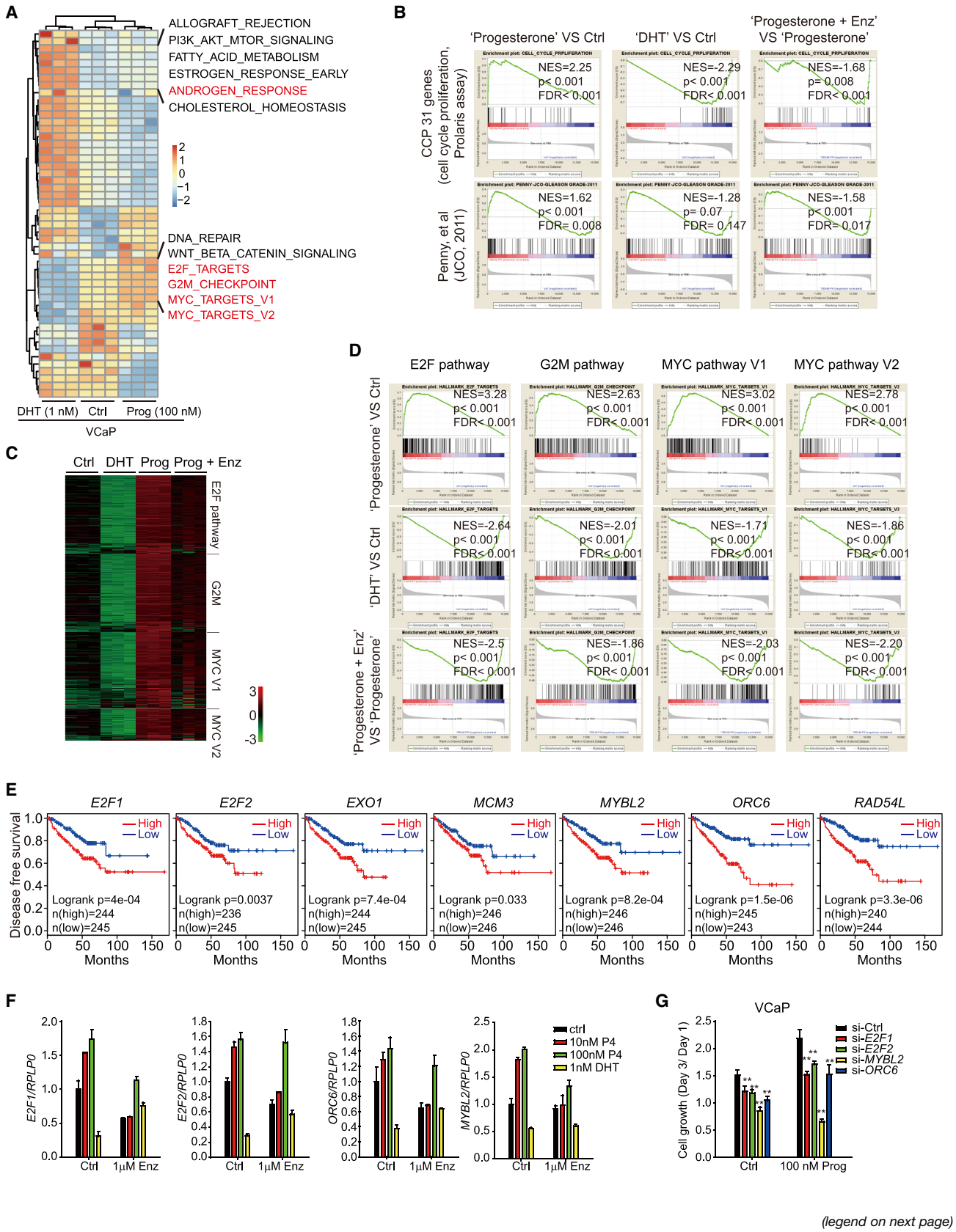

(legend on next page)

AR^{H875Y}; these effects were not observed in cells expressing AR^{W742L} (Figures 1K and 1L). Xenografts generated from LAPC4-AR^{H875Y} cells grew more rapidly with progesterone treatment (Figure 1M). Together, these data indicate that patients with AR^{T878A} or AR^{H875Y} may be more sensitive to the oncogenic effects of progesterone.

Non-canonical AR target genes regulated by progesterone

Transcriptome analysis of VCaP cells revealed that progesterone and DHT differentially regulated several pathways, according to molecular signatures database (MSigDB) hallmark gene set collection (Figure 2A; Table S4).[23] Different gene signatures have been developed to indicate the aggressiveness of prostate cancer, including the 31-gene signature of cell cycle progression (CCP) and 157-gene signature of Gleason grade.[24,25] These signatures were both enriched after progesterone treatment, but not DHT treatment, consistent with previous observation (Figure 2B) .[26] Notably, although AR signaling was enriched after progesterone treatment in VCaP cells, the most significant pathways upregulated by progesterone were E2F, G2M, and MYC-related pathways, which were suppressed by DHT. Enzalutamide suppressed the function of progesterone on these pathways, indicating the involvement of AR (Figures 2C and 2D). Thus, we recognize these progesterone-activated but DHT-repressed genes as non-canonical AR target genes. Gene expression profiling interactive analysis (GEPIA) revealed that patients with active expression of these non-canonical AR target genes had a shorter treatment duration (Figure 2E).[27] The regulation of non-canonical AR target genes by progesterone was further confirmed by quantitative PCR (qPCR) in VCaP cells (Figure 2F).[27] However, knockdown of PR cannot consistently deregulate the expression of non-canonical AR target genes in VCaP cells (Figure S2L). Knockdown of these non-canonical AR target genes suppressed the proliferation of VCaP cells (Figure 2G). Together, these data demonstrate that progesterone promotes prostate cancer progression via AR through regulation of canonical and non-canonical target genes.

Oncogenic effects of progesterone at the physiological level

The transient oncogenic effects of progesterone were observed at a dose of 10–100 nM. Although the dosage was achievable in patients after abiraterone treatment, most abiraterone-treated patients (38 out of 47; 80.85%) obtained a plasma concentration lower than 10 nM (Figure 1C). The correlation between plasma progesterone concentrations and poor clinical outcomes indicated an oncogenic effect of progesterone at physiological levels. Patients treated with abiraterone experienced long-term stimulation from progesterone, which may result in irreversible alterations in the transcriptome of cancer cells. Thus, LAPC4 cells, with limited response to the transient treatment of progesterone, were treated with 5 nM progesterone or ethanol for 6 months to generate Prog_cells and Ctrl_cells, respectively.

Prog_cells exhibited higher proliferation than Ctrl_cells, even when treated with no additional steroids, including progesterone (Figure 3A). Interestingly, transient treatment with progesterone did not promote the growth of Prog_cells or Ctr_cells (Figure S3A). Transcriptome analysis revealed an activated estrogen response pathway in Prog_cells, while the expression of AR, estrogen receptor 1 (ESR1), and PR was not changed in the Prog_cells (Figure 3B, 3C, S3B, and S3C). Knockdown of PR showed no effect on cell proliferation in Prog_cells (Figure S3D). These genes, which are involved in the estrogen response pathway, were further analyzed using different databases (Figure 3D).[28,29] Frequent amplification of these genes in prostate cancer and increasing expression as the disease progresses were discovered (Figures S3E and S3F). Higher expression of these genes was correlated with worse clinical outcomes in prostate cancer patients (Figure S3G). The active expression of genes involved in the estrogen response pathway was further confirmed by qPCR of Prog_cells (Figure 3E). Knockdown of these genes suppressed cell proliferation (Figure 3F). Together, these data suggest that the physiological levels of progesterone have accumulating oncogenic effects in prostate cancer.

Transcriptional factors that mediate the accumulating oncogenic effects of progesterone were investigated. Eighty-seven leading-edge genes of the estrogen response pathway were selected for potential transcriptional factor prediction using the ChEA3 Website.[30] The predicted transcriptional factors were further evaluated based on the gene expression in Prog_cells and survival correlation using GEPIA (Figure 3G). GATA2 was the only qualified transcriptional factor identified after this bioinformatic screening. Frequent gene amplification of GATA2 and a positive correlation with treatment failure were found in prostate cancer (Figures S4A and S4B). A positive correlation between GATA2 and genes involved in the estrogen response pathway in gene expression was also observed (Figures S4C and S4D). The increase of GATA2 in Prog-cells was further confirmed at the mRNA and protein levels (Figures 3H and 3I). The GATA2 inhibitor, K7174, inhibited the expression of genes involved in the estrogen response pathway in Prog_cells (Figure 3J).[31] The function of K7174 was more significant in Prog_cells than in Ctrl_cells in regulating gene expression (Figure 3K). K7174 also suppressed cell proliferation more

Figure 2. The non-canonical AR target genes regulated by progesterone

(A) Heatmap of pathway analysis in VCaP cells. Gene set variation analysis (GSVA) was performed according to Hallmark GeneSet.

(B) Enrichment of aggressiveness associated gene signatures in progesterone-treated VCaP cells.

(C) Genes upregulated by progesterone but not DHT on VCaP cells. RNA-seq was performed in VCaP cells. Enz, enzalutamide, 1 μM; DHT, 1 nM; Prog, 100 nM.

(D) GSEA on the progesterone-regulated non-canonical AR target genes.

(E) Correlation between progesterone-regulated non-canonical AR target genes and poor clinical outcomes analyzed via GEPIA.

(F) Regulation of the progesterone-activated non-canonical AR target genes in VCaP cells.

(G) Effects of the progesterone-activated non-canonical AR target genes on cell proliferation in VCaP cells. Technical replicate (n = 2) for qPCR; biological replicate (n = 5) for cell proliferation assay (see also Figure S2L; Table S4).

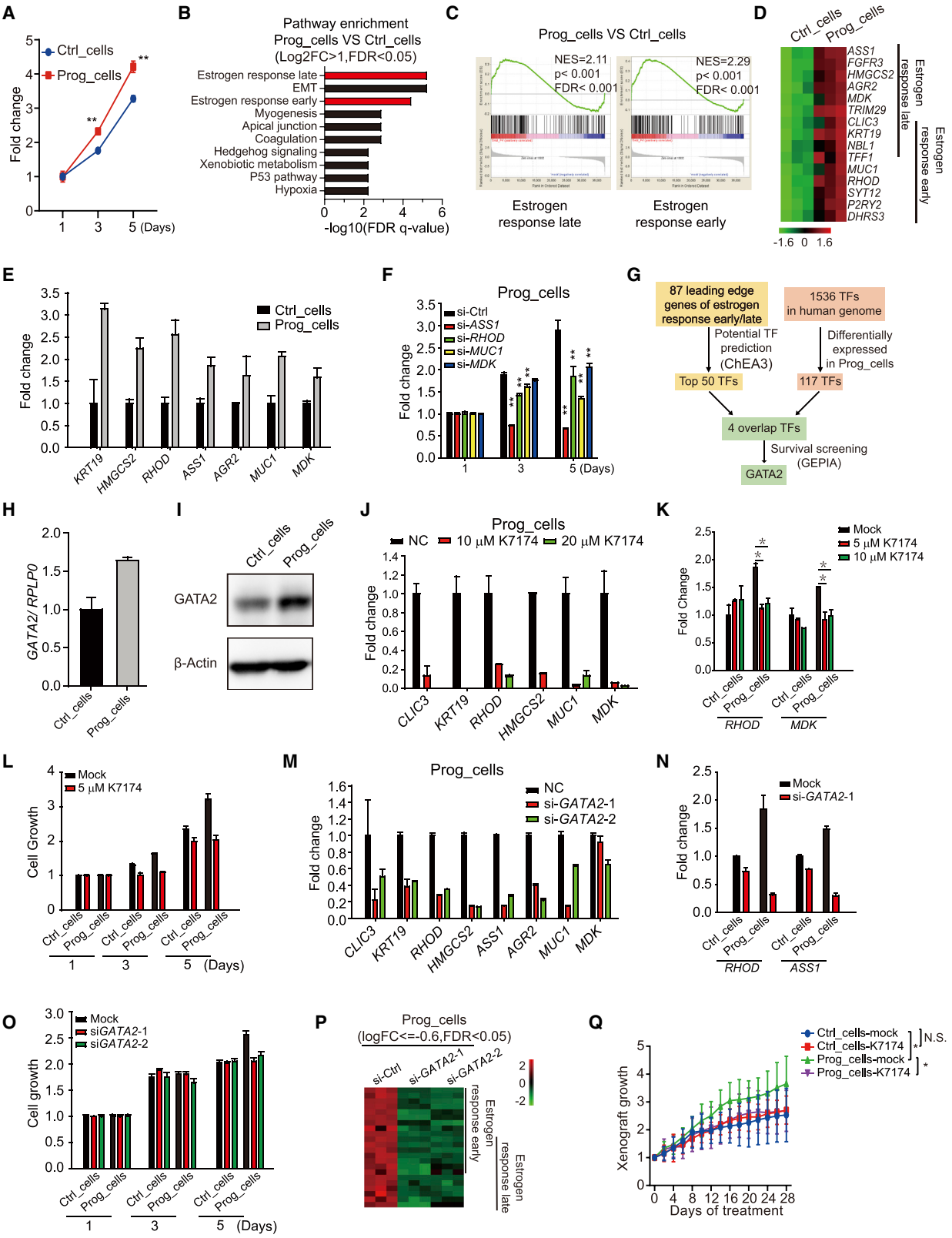

(legend on next page)

dramatically in Prog_cells (Figure 3L). GATA2 was also knocked down using different small interfering RNAs (siRNAs) (Figure S4E). The expression of genes involved in the estrogen response pathway was impaired by GATA2 knockdown (Figure 3M). The effect of GATA2 knockdown on gene expression and cell proliferation was more pronounced in Prog_cells (Figures 3N and 3O). Transcriptome analysis also revealed that siRNAs targeting GATA2 suppressed the estrogen response pathway in Prog_cells (Figure 3P; Figures S4F and S4G). Xenografts generated from the Prog_cells grew more rapidly than xenografts generated from the Ctrl_cells. The GATA2 inhibitor K7174 specifically suppressed Prog_cell-generated xenograft growth (Figure 3Q). Together, these data demonstrate that GATA2 mediates the accumulating oncogenic effects of progesterone and is a potential target for prostate cancer treatment.

Targeting progesterone metabolism to halt the oncogenic effects of progesterone

Suppressing the generation of progesterone provides a potential strategy to eliminate the transient and accumulating oncogenic effects of progesterone. Pregnenolone, generated from cholesterol, is converted to progesterone by 3β-hydroxysteroid dehydrogenase 1/2 (3βHSD1/2).[2] Based on our knowledge of steroidal metabolism, we hypothesized that progesterone is converted to 5α-progesterone (5αP), 5β-progesterone (5βP), and the related downstream metabolites in patients (Figure 4A).[32–34] Pregnenolone, progesterone, and 5αP were used to treat LNCaP cells to confirm the progesterone metabolic pathway (Figure S5A). [^{3}H]-pregnenolone was used to treat fresh patient prostate biopsy samples *ex vivo*. Pregnenolone was actively converted to progesterone and 5αP in biopsy samples (Figure 4B).[35] The distribution of progesterone-related metabolites was also investigated with plasma samples from seven abiraterone-treated patients to show that pregnenolone, progesterone, and 5αP were the main metabolites found in patients (Figure S5B). The function of these metabolites was further investigated, and we found that most metabolites activated AR signaling in LNCaP and VCaP cells (Figure 4C). Pregnenolone, progesterone, and 5αP activated AR target gene expression in a dose-dependent manner (Figure S5C). The docking model indicated that pregnenolone, progesterone, and 5αP bound to the ligand-binding domain of AR comparably (Figure S5D).[36,37] However, the 3α-OH-Δ-5 structure of pregnenolone is not an ideal ligand for the AR. Competition assays were performed on LNCaP and VCaP cells using all progesterone-related metabolites, and results showed that progesterone and 5αP had the most potent affinity for the AR (Figure S5E). Pregnenolone exhibited limited binding affinity for wild-type AR and the AR^{T878A} mutant (Figure 4D). Thus, the oncogenic function of pregnenolone might result from its conversion to progesterone. This hypothesis was further validated using mouse tissues. Mouse prostate tissue showed no 3βHSD1/2 activity and converted no DHEA to AD (Figure 4E).[2,35] Prostate organoids generated from *Pb*$^{Cre/+}$ *Pten*$^{flox/flox}$ mice could not convert pregnenolone and DHEA to downstream metabolites (Figure 4F).[2,38] Thus, pregnenolone did not enhance the formation of prostate organoids as progesterone (Figure 4G). Pregnenolone was not capable of activating AR signaling in the mouse prostate organoids (Figure 4H). Together, these data indicate that inhibiting the conversion of pregnenolone to progesterone is a potential strategy for prostate cancer treatment.

The adrenal gland is not the only source for pregnenolone and progesterone.[39,40] The periprostatic adipose tissue might also contribute steroids to prostate cancer cells through paracrine mechanisms. Fresh periprostatic adipose tissues were collected from seven prostate cancer patients receiving radical prostatectomy and cultured in DMEM for 2 days. The secretion of adipose tissues from three patients activated AR target genes in LNCaP

Figure 3. The accumulating oncogenic effects of progesterone via GATA2

(A) Enhanced proliferation potential in Prog_cells. Prog_cells, LAPC4 cells treated with 5 nM progesterone for more than 6 months. Ctrl_cells, LAPC4 cells treated with ethanol for more than 6 months. No extra steroids, including progesterone, were added for the proliferation assay.

(B) Pathway enrichment in Prog_cells. Transcriptome analysis of Prog_cells (without transient progesterone stimulation) and Ctrl_cells was performed.

(C) GSEA of the estrogen response pathway in Prog_cells and Ctrl_cells.

(D) Heatmap of the estrogen response signature genes in Prog_cells.

(E) Expression levels of the estrogen response signature genes in Prog_cells. Gene expression was determined in Prog_cells and Ctrl_cells without transient stimulation of progesterone.

(F) Effects of the estrogen response signature genes on Prog_cells proliferation. Cell proliferation assays were performed without extra steroids, including progesterone.

(G) Schema of transcription factor screening. Potential transcription factors involved in the estrogen response pathway in Prog_cells were screened. TF, transcription factor.

(H and I) GATA2 expression in Prog_cells. mRNA and protein levels of GATA2 in Prog_cells and Ctrl_cells were determined.

(J) Effect of a GATA2 inhibitor on the expression of estrogen response signature genes. The GATA2 inhibitor K7174 was used to treat Prog_cells for 24 h.

(K) Effects of the GATA2 inhibitor on gene expression in Prog_cells and Ctrl_cells.

(L) Effects of the GATA2 inhibitor on cell proliferation. Prog_cells and Ctrl_cells were treated with K7174 for cell proliferation assays.

(M) Gene expression in Prog_cells after GATA2 knockdown.

(N) Gene expression in Prog_cells and Ctrl_cells after GATA2 knockdown.

(O) Cell proliferation in Prog_cells and Ctr_cells after GATA2 knockdown.

(P) Heatmap of estrogen response signature genes after GATA2 knockdown in Prog_cells. GATA2 was knocked down using different siRNAs in Prog_cells before transcriptome analysis.

(Q) Effect of the GATA2 inhibitor on xenograft growth. Xenografts were generated from Ctrl_cells and Prog_cells, respectively, and treated with K7174 (25 mg/kg). Ten mice for every group. Results are represented as means ± SD. Experiments were performed at least three times independently. Technical replicate (n = 2) for qPCR; biological replicate (n = 5) for cell proliferation assay. *p < 0.05 (see also Figures S3 and S4).

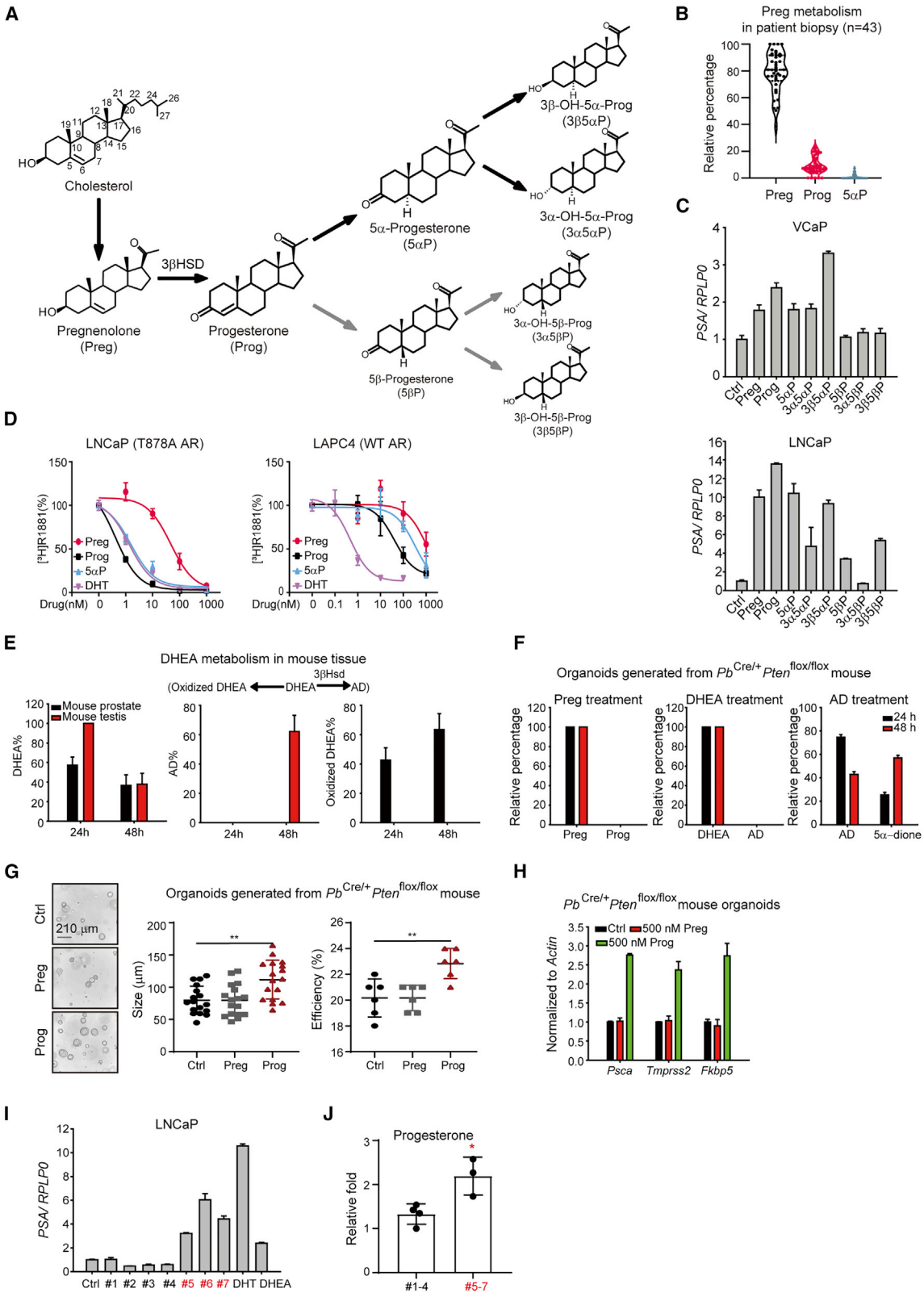

(legend on next page)

cells (Figure 4I). Significantly higher concentrations of pregnenolone were detected in the secretion of these AR-activating adipocyte tissues (Figure 4J). These results indicate that the effects of pregnenolone are not limited to abiraterone-treated patients.

To inhibit the conversion of pregnenolone to progesterone, steroidogenic enzyme 3βHSD1 is a promising target (Figure 4A).[35] Currently, there is no 3βHSD1 inhibitor available in clinic. To discover novel 3βHSD1 inhibitors, a virtual screening was conducted with a previously reported spliced 3βHSD1 structure model.[37,41] Corylin, a flavonoid reported to have anti-inflammatory and anti-cancer activity at a high dose (>10 μM), was found to be a potential candidate to bind to 3βHSD1 in our virtual screening system.[42] Coincidently, mouse 3βHsd3/3βHsd5, with high similarity to human 3βHSD1, were pulled down by a photo-crosslinking probe of corylin in our previous work.[43] Thus, the effect of corylin on human 3βHSD1 was tested. Corylin inhibited the conversion of DHEA to AD dose dependently (Figure 5A). Corylin derivatives were further screened, and biochanin A (BCA) was identified as the most potent 3βHSD1 inhibitor (Figures 5B and 5C). To determine the potential interaction between BCA and 3βHSD1, cellular thermal shift assay (CETSA) was performed and BCA increased the thermal stability of 3βHSD1, similar to DHEA (Figure 5D).[44] A BCA probe was synthesized and its function in suppressing 3βHSD1 activity was confirmed (Figures 5E and 5F). Purified glutathione S-transferase (GST)-3βHSD1 was pulled down by this BCA probe *in vitro*. The addition of DHEA or BCA interrupted the binding of the BCA probe to GST-3βHSD1 (Figure 5G). Consistently, the docking model with the spliced 3βHSD1 structure also indicated that BCA competed with DHEA to bind to the substrate recognition pocket of 3βHSD1 (Figure 5H).[37] Essential amino acids of 3βHSD1 involved in BCA binding were predicted according to the docking results and mutated for enzyme activity assays. The E126A mutant impaired BCA function completely, indicating the important role of E126 in recognizing BCA (Figure 5I). Together, these data demonstrate that BCA directly and potently suppresses the activity of 3βHSD1.

The specificity of BCA as a 3βHSD1 inhibitor in biological functions was also evaluated. BCA specifically inhibited DHEA- but not DHT-induced AR target gene expression (Figure 5J). Transcriptome analysis of VCaP cells revealed that AR target genes were specifically regulated by BCA (Figures S5F–S5H). BCA, alone at a dose of 1 μM, affected limited genes or no pathways in VCaP, PC3, and LNCaP cells (Figures S6A and S6B). Furthermore, BCA at a dose of less than 10 μM, had no effect on the proliferation of AR-negative PC3 cells (Figure S6C). These data together support the specificity of BCA, at a dose of less than 10 μM, as a 3βHSD1 inhibitor.

To determine the function of BCA in regulating progesterone synthesis, a VCaP cell line stably expressing Dox-induced 3βHSD1 was treated with pregnenolone with or without BCA. The conversion from pregnenolone to progesterone was accelerated by 3βHSD1 overexpression but reduced by BCA (Figure 5K). By suppressing the conversion of pregnenolone to progesterone, BCA successfully suppressed pregnenolone-induced gene expression and cell proliferation in VCaP and LNCaP cells, but showed no effect on progesterone (Figures 5L–5N). Pregnenolone and progesterone facilitated the growth of xenografts generated from C4-2 cells in castrated mice. BCA successfully suppressed pregnenolone- but not progesterone-sustained xenograft development (Figure 5O). Together, these data demonstrate that inhibiting the synthesis of progesterone is a feasible strategy to halt the oncogenic effects of progesterone.

Progesterone as a predictive biomarker for abiraterone response

Based on its oncogenic effects, progesterone might be a predictive biomarker for abiraterone response if the increase in plasma progesterone is an early event after abiraterone treatment. The clinical information of abiraterone-treated patients was re-examined (Table S5). A total of 17 CRPC patients had plasma progesterone detected at baseline, 3 months after abiraterone treatment, and at the endpoint. An increase in plasma levels of progesterone was observed in these 17 patients after 3 months of abiraterone treatment (Figure 6A). Patients with higher plasma levels of progesterone at the endpoint had higher plasma levels of progesterone after 3 months of abiraterone treatment (Figure 6B). These data together confirm the early onset of an increase in plasma progesterone levels in abiraterone-treated patients.

Figure 4. Function of progesterone-related metabolites in prostate cancer

(A) Schema of progesterone metabolism in prostate cancer cells. Gray arrows indicate potential progesterone metabolism in the liver.

(B) Pregnenolone metabolism in patient biopsy samples. [^{3}H]-pregnenolone was used to treat biopsy samples from prostate cancer patients.

(C) Effects of progesterone and other metabolites on AR target gene in VCaP and LNCaP cells. Cells were treated with 1 μM progesterone or related metabolites before PSA detection.

(D) Affinity of progesterone and other metabolites to the AR. Progesterone and other metabolites at different doses were used to compete with 1 nM [^{3}H]-R1881 in LNCaP cells (expressing AR^{T878A} mutant) and LAPC4 cells (expressing wild-type AR).

(E) Lack of 3βHSD activity in mouse prostate tissue. Fresh tissues from mouse prostate and testis were minced and transiently cultured with [^{3}H]-DHEA. AD, androstenedione.

(F) Lack of 3βHSD activity in the prostate organoids. Prostate organoids were generated from 3-month-old *Pb*$^{Cre/+}$ *Pten*$^{flox/flox}$ mice and treated with [^{3}H]-pregnenolone, [^{3}H]-DHEA, or [^{3}H]-AD.

(G) Effects of pregnenolone and progesterone on organoids formation. Pregnenolone, 500 nM; progesterone, 500 nM. Organoids were generated with prostate gland from *Pb*$^{Cre/+}$ *Pten*$^{flox/flox}$ mouse.

(H) Effects of pregnenolone and progesterone on Ar target gene expression in *Pb*$^{Cre/+}$ *Pten*$^{flox/flox}$ mouse prostate organoids.

(I) Secretions of periprostatic adipocyte tissues activated AR signaling in LNCaP cells. Periprostatic adipocyte tissues from seven patients were collected and incubated in DMEM + 10% FBS for 2 days. This medium was utilized to treat LNCaP cells. DHEA, 40 nM; DHT, 0.1 nM.

(J) Relative fold of progesterone in the secretions of periprostatic adipocyte tissues. Results are represented as means ± SD. Experiments were performed at least three times independently. Technical replicate (n = 2) for qPCR; biological replicate (n = 3) for organoids assay (see also Figures S5A–S5E).

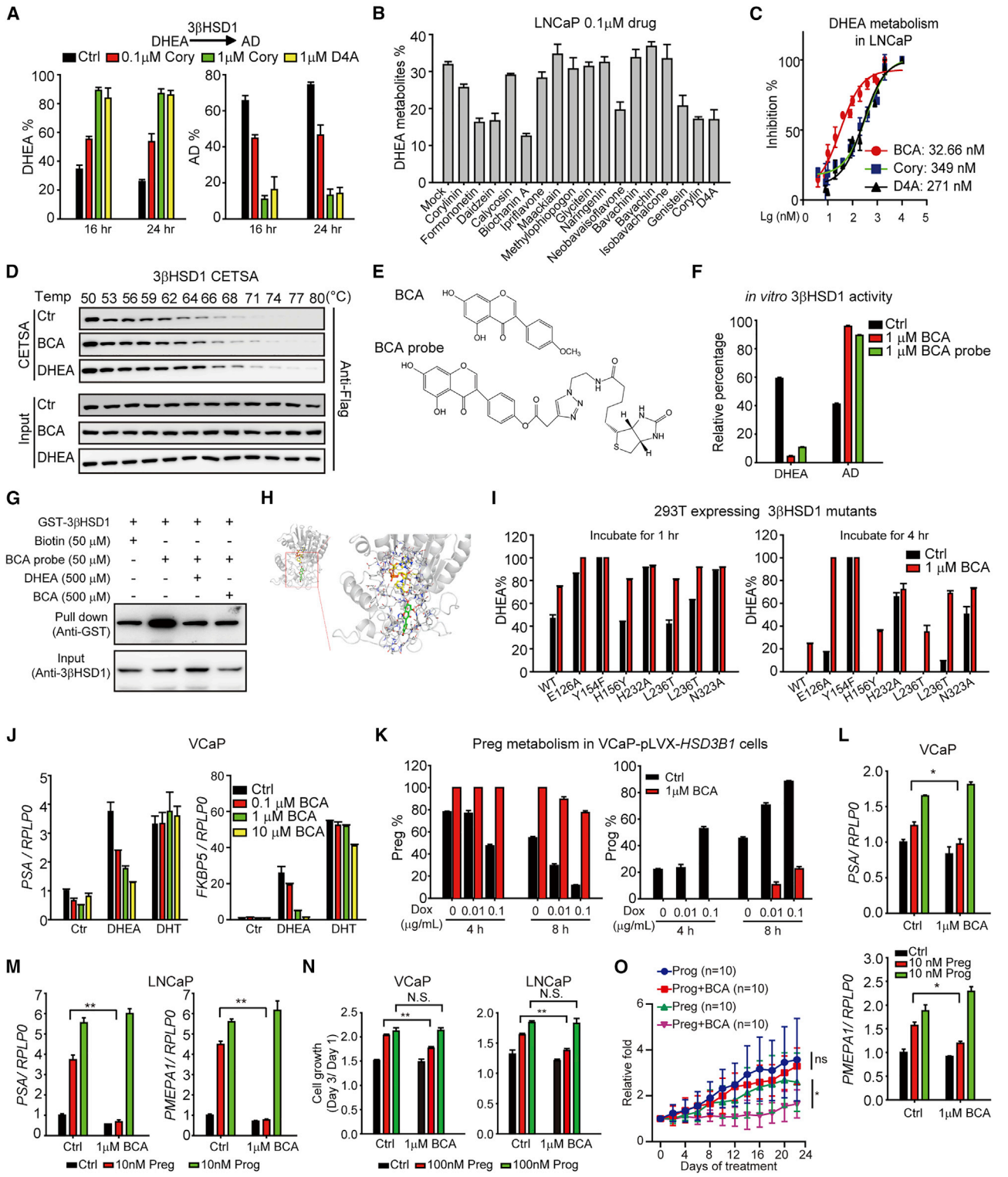

Figure 5. BCA eliminates the oncogenic effects of progesterone as an inhibitor of 3βHSD1

(A) Corylin inhibited DHEA conversion to AD. Cells were treated with [^{3}H]-DHEA and the indicated drugs. The percentage of DHEA and downstream metabolites was calculated. Cory, corylin; AD, androstenedione.

(B) Effect of corylin derivatives on DHEA metabolism.

(C) BCA significantly inhibited DHEA metabolism. LNCaP cells were treated with drugs with the indicated doses and [^{3}H]-DHEA. BCA, biochanin A.

(legend continued on next page)

The predictive role of plasma progesterone levels was further investigated. Patients with plasma concentrations >3 nM after 3 months of abiraterone treatment had a shorter abiraterone treatment duration (Figure 6C). PSA reduction after 3 months of abiraterone treatment is frequently used in clinic to evaluate patient response. In 11 out of 17 CRPC patients, a PSA reduction more than 50% from the baseline was identified (Figure 6D).[45] Patients with a more significant PSA reduction had a lower plasma progesterone concentration after 3 months of abiraterone treatment (Figure 6E). We further expanded the analysis to all abiraterone-treated patients, including both CRPC and HSPC patients. The predictive role of progesterone was also confirmed in these patients (Figure S7). Together, these data indicate the potential of plasma progesterone levels as a predictive biomarker for abiraterone response.

DISCUSSION

Metabolites beyond androgens may drive the progression of prostate cancer. The discovery of these oncometabolites could provide novel insights into disease management. Here, we performed UHPLC-MS screening and retrospective analysis on clinical data to identify progesterone as an oncogenic hormone in prostate cancer. The investigation on the oncogenic effects of progesterone provided potential targets, including AR, GATA2, and 3βHSD1, for further disease management.

The oncogenic effects of other metabolites may be concealed by androgens. ADT and abiraterone together eliminate the major androgen resources from the testis and adrenal glands, providing a relatively clear background to discover novel oncometabolites. Progesterone is considered a female hormone involved in the menstrual cycle. It binds to the PR and regulates fetus implantation and other essential physiological functions.[46] Progesterone and the PR have been reported as preventive factors in breast, colon, and lung cancer.[47–49] Patients with low progesterone levels had a higher risk of premenopausal breast cancer and overall mortality.[50] However, the enthusiasm for investigating progesterone in prostate cancer is limited due to the trace amount of endogenous progesterone in men. Abiraterone significantly increased the plasma concentration of progesterone, providing a unique scenario for progesterone to exert its oncogenic effect.

The oncogenic effects of progesterone in prostate cancer may be PR independent. PR is expressed mainly in stromal cells but not in epithelial cells in the prostate.[51] PR might regulate stromal cells and indirectly inhibit prostate cancer, independent of progesterone.[51] Progesterone has been reported to inhibit benign prostatic hyperplasia and prostate cancer, possibly due to its effects on SRD5A and pituitary luteinizing hormone (LH) release.[52] However, in patients receiving ADT and abiraterone, the significance of SRD5A and LH release may not be essential.[53,54] Recently, the progesterone-responsive AR^{T878A} mutant was identified in abiraterone-treated patients, indicating a potential progesterone-related resistance mechanism.[10]

A high dose of progesterone bound to the AR directly, and its affinity to AR was dependent on the AR genotype.[55] Thus, patients with AR^{W742L} and AR^{M750T} are more suitable for abiraterone treatment than patients expressing AR^{T878A} and AR^{H875Y}. Progesterone has a relatively mild affinity for wild-type AR, and increasing AR abundance magnifies the oncogenic effect of progesterone, consistent with the clinical observation of AR expression after abiraterone treatment.[56] Progesterone also uniquely regulates the expression of non-canonical AR target genes. These non-canonical genes are involved in the cell cycle and gene transcriptional regulation, which are essential for cell survival. Previous reports also revealed different AR signatures activated by different ligands or drugs, supporting the context-specific function of AR in prostate cancer.[57,58]

More than 10 nM progesterone is needed to activate AR signaling, and only 9 out of 47 (19.15%) patients achieved this dose after abiraterone treatment in this study. Unlike the cell lines with a transient treatment of progesterone, abiraterone-treated patients encounter persistent progesterone stimulation in their daily lives. Long-term stimulation of progesterone might result in irreversible alterations in the genome or transcriptome of prostate cancer cells.[10] LAPC4 cells were not sensitive to transient progesterone treatment due to their low AR expression. However, a more aggressive LAPC4 cell line was generated after treatment with physiological levels of progesterone for more than 6 months. Genes involved in the activated estrogen response

(D) BCA increased the thermal stability of 3βHSD1. BCA or DHEA was added to FLAG-3βHSD1-expressing cells. Cell lysates were incubated at different temperatures to determine the stability of 3βHSD1. BCA, 20 μM; DHEA, 20 μM.
(E) Structure of the BCA-biotin probe.
(F) The BCA probe inhibited 3βHSD1 activity. GST-3βHSD1 (3 μg) was used for the *in vitro* enzyme activity assays. BCA, 1 μM; BCA probe, 1 μM.
(G) The BCA probe directly bound to GST-3βHSD1. GST-3βHSD1 (3 μg) was incubated with the BCA probe with or without DHEA or BCA for pull-down assays.
(H) Docking of BCA with the previously reported 3βHSD1 model. BCA, green. NAD, yellow. Hydrogen atoms, white; oxygen atoms, red; nitrogen atoms, blue; phosphor atoms, orange.
(I) Amino acids of 3βHSD1 essential for the function of BCA. Plasmids with different amino acids mutated were transfected in 293T cells for DHEA metabolism assays.
(J) BCA inhibited DHEA-induced AR target gene expression. VCaP cells were treated with the indicated drugs. DHEA, 100 nM; DHT, 1 nM.
(K) Inhibition of progesterone generation by 3βHSD1 inhibitor BCA. VCaP-pLVX-*HSD3B1*, a stable cell line with Dox-induced 3βHSD1 expression in VCaP cells.
(L) BCA suppressed pregnenolone-induced gene expression in VCaP cells.
(M) BCA suppressed pregnenolone-induced gene expression in LNCaP cells. Pregnenolone and progesterone were used to treat LNCaP cells with or without BCA.
(N) BCA suppressed pregnenolone-induced cell proliferation.
(O) BCA suppressed pregnenolone- but not progesterone-induced xenograft growth. Xenografts were generated with C4-2 cells. BCA, 50 mg/kg. Results are represented as means ± SD. Experiments were performed at least three times independently. Technical replicate (n = 2) for qPCR; biological replicate (n = 3) for metabolism assay. *$p < 0.05$; **$p < 0.01$ (see also Figures S5F–S5H and S6).

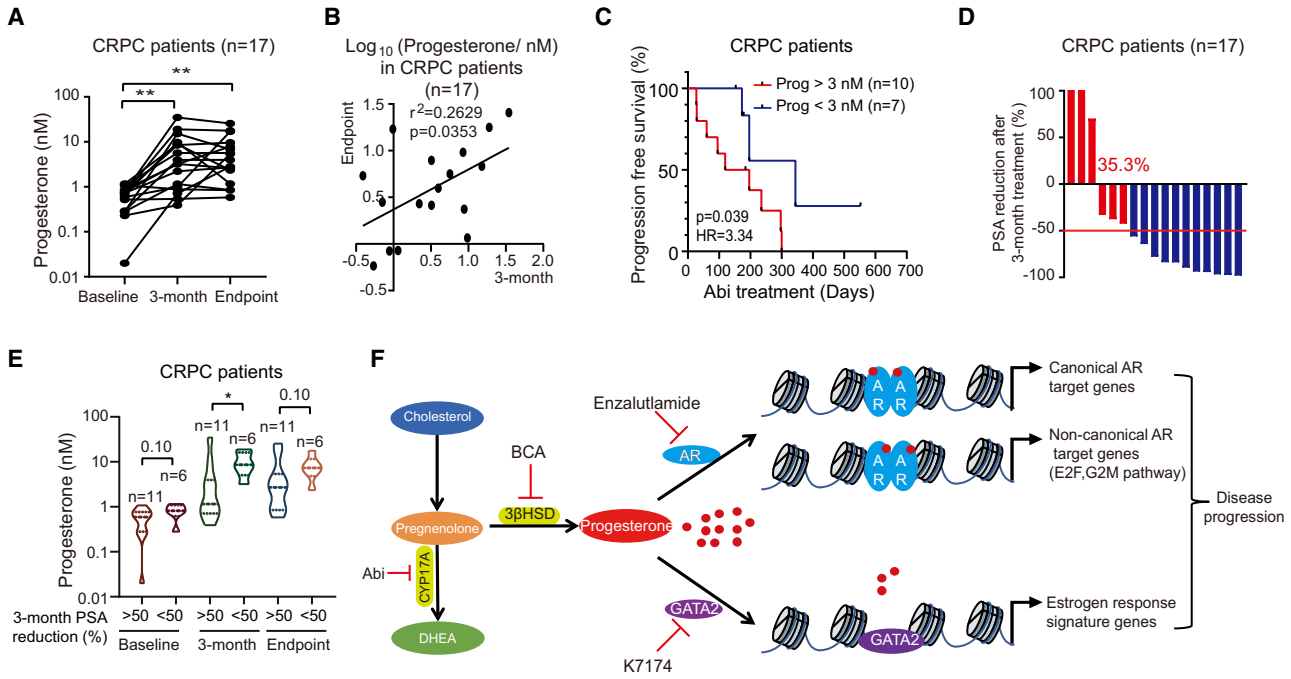

Figure 6. Progesterone as a predictive biomarker for the response to abiraterone treatment

(A) Alterations of plasma progesterone concentrations in CRPC patients. Progesterone concentrations at different time points (baseline, 3 months after abiraterone treatment, and endpoint) were compared. Alterations in plasma progesterone in the same patient are linked with lines.

(B) Correlation between plasma progesterone levels after 3 months of abiraterone treatment and that at the endpoint in CRPC patients. Pearson correlation for p values.

(C) Higher plasma progesterone as a risk indicator for shorter treatment duration in CRPC patients. Plasma concentrations of progesterone in patients after 3 months of abiraterone treatment were used to predict clinical outcomes. Progression was determined via PSA according to PCWG2 guidelines.

(D) PSA response in CRPC patients after 3 months of abiraterone treatment.

(E) Comparison of plasma progesterone levels in CRPC patients. Patients were stratified by PSA response after 3 months of abiraterone treatment.

(F) Graph illustrating the oncogenic effects of progesterone in abiraterone-treated patients (see also Figure S7; Table S5).

pathway, including *MUC1*, *MDK*, and *HMGCS2*, have been reported to promote neuroendocrine prostate cancer (NEPC) progression,[59,60] maintain the stemness of prostate cancer,[61] and promote disease progression,[62] indicating a potential role of progesterone to promote NEPC progression. GATA2 mediated the activation of the estrogen response pathway. GATA2 was reported to be a pioneer transcription factor that facilitates nuclear receptor recruitment.[63,64] The positive correlation between GATA2 and prostate cancer has been clarified and validated.[65,66] K7174, a GATA2 inhibitor, inhibited the accumulating effect of progesterone in Prog_cells, providing a potential strategy for prostate cancer management after abiraterone resistance.

The analysis of progesterone metabolism and the function of progesterone-related metabolites revealed that 3βHSD1 is an ideal target to eliminate the oncogenic effects of progesterone. Enzalutamide and K7174 only restrained the transient and accumulating oncogenic function of progesterone, respectively. Since pregnenolone shows limited effects on prostate cancer cells, inhibiting 3βHSD1 to suppress the conversion from pregnenolone to progesterone is a more promising strategy. Although the clinical significance of 3βHSD1 has been intensively investigated only recently, there is no available 3βHSD1 antagonist in clinic. Here, we identified BCA as a potent 3βHSD1 inhibitor and showed that BCA suppressed the generation and function of progesterone. Aside from progesterone metabolism, 3βHSD1 also participates in abiraterone and DHEA metabolism to facilitate drug clearance and androgen accumulation.[2,67] Thus, 3βHSD1 is a promising target for enhancing the clinical efficacy of abiraterone.

Reliable biomarkers are required for patient stratification and personalized medicine.[68] Currently, there are limited criteria to identify patients who are suitable for abiraterone treatment. We found that the plasma level of progesterone is a potential predictive biomarker of abiraterone response. Patients showing a significant increase in progesterone levels might benefit more from enzalutamide than abiraterone, especially for those expressing AR^{T878A} or AR^{H875Y} mutants. The increase in plasma progesterone levels might also reflect the potency of 3βHSD1 in patients. Abiraterone inhibits CYP17A, leading to the accumulation of pregnenolone and progesterone. 3βHSD1 catalyzes pregnenolone to generate progesterone. Patients with higher plasma levels of progesterone after abiraterone treatment might have more potent activity of 3βHSD1, which has been reported as a risk factor of treatment failure.[69,70] However, the patients enrolled in this real-world analysis were not as rigorously examined as patients enrolled in clinical trials, and the patient number should be increased to confirm the role of progesterone as a predictive biomarker for the response to abiraterone.

In summary, this work identified progesterone as an oncogenic hormone in prostate cancer patients receiving abiraterone treatment. BCA was discovered as a potent 3βHSD1 inhibitor and prevented the oncogenic effects of progesterone by suppressing the synthesis of progesterone. Higher plasma levels of progesterone are correlated with poor clinical outcomes of abiraterone treatment in patients (Figure 6F).

Limitations of the study

The limitations of our study include limited cell lines used for the chronic effects of progesterone. The detailed mechanisms for BCA to inhibit 3βHSD1 need to be further determined. The oncogenic effect and predictive biomarker role of serum progesterone should be further validated in a large cohort of patients.

STAR★METHODS

Detailed methods are provided in the online version of this paper and include the following:

- KEY RESOURCES TABLE
- RESOURCE AVAILABILITY
  - Lead contact
  - Materials availability
  - Data and code availability
- EXPERIMENTAL MODEL AND SUBJECT DETAILS
  - Patients
  - Cell lines
  - Animal models
- METHOD DETAILS
  - Reagents
  - Preparation of standard solutions for calibration curves
  - Preparation of plasma samples
  - Derivatization of sterol metabolites with 2-Picolinic acid
  - UHPLC-MS/MS analysis
  - Untargeted metabonomics analysis with UPLC-QTOFMS
  - Detection of plasma progesterone and its metabolites
  - Chemical compounds
  - Steroidogenesis in patient biopsy samples
  - Mouse prostatic organoids
  - HPLC
  - Effects of periprostatic adipose tissue medium
  - Gene expression
  - Cell proliferation assay
  - Immunoblotting
  - Immunofluorescence
  - AR competition assay
  - Luciferase reporter gene assay
  - Mouse xenograft studies
  - BCA probe pull-down assay
  - CETSA
  - Computational biochemistry
- QUANTIFICATION AND STATISTICAL ANALYSIS
  - RNA-seq
  - Pathway enrichment and gene set enrichment analysis
  - Statistics

SUPPLEMENTAL INFORMATION

Supplemental information can be found online at https://doi.org/10.1016/j.xcrm.2022.100561.

ACKNOWLEDGMENTS

We thank our patients and their families. We thank the staff members (Zhuo Yang et al.) of the chemical biology core facility in Shanghai Institute of Biochemistry and Cell Biology, staff members (Chao Peng et al.) of mass spectrometry at the National Facility for Protein in Shanghai (NFPS)/Shanghai Advanced Research Institute, and staff members (Pengyu Wang et al.) of Bio-Med Big Data Center/Shanghai Institute of Nutrition and Health for their support. This work is supported by the National Key R&D program of China (2018YFA0508200), the National Natural Science Foundation of China (92157101, 31771575, 31821002, 81590953, and 81872075), Ministry of Science and Technology of China (2018YFE0201603, 2020YFE0201600, and 2017YFC0906800), New Frontier Technology Joint Research Project of Shanghai Municipal Hospital (SHDC12019112), Natural Science Foundation of Shanghai (21ZR1458300), Shanghai Municipal Science and Technology Major Project (2017SHZDZX01), a Prostate Cancer Foundation Young Investigator Award, and the Science, Technology, and Innovation Commission of Shenzhen Municipality (JCYJ-20210324124611031).

AUTHOR CONTRIBUTIONS

Conceptualization, Z.L.; methodology, L.C., H.T., and Y.G.; investigation, Z.H., S.H., Z.M., J.G., Q.Z., X.Z., Q.T., T.Y., Y.L., Y.C., D.W., T.J., X.S., Y.W., R.R., L.Q., X.X., and J.Q.; writing, Z.L., H.T., D.W., Z.H., S.H., and Z.M.; funding acquisition, Z.L., D.W., H.T., and R.R.; resources, S.H., D.W., T.J., and X.S.; supervision, Z.L., H.T., and D.W.

DECLARATION OF INTERESTS

The authors declare no competing interests.

Received: November 7, 2021
Revised: January 17, 2022
Accepted: February 16, 2022
Published: March 15, 2022

REFERENCES

1. Sharifi, N., and Auchus, R.J. (2012). Steroid biosynthesis and prostate cancer. Steroids *77*, 719–726.
2. Hou, Z., Huang, S., and Li, Z. (2021a). Androgens in prostate cancer: a tale that never ends. Cancer Lett. *516*, 1–12.
3. Auchus, R.J., and Sharifi, N. (2020). Sex hormones and prostate cancer. Annu. Rev. Med. *71*, 33–45.
4. Huggins, C. (1946). Prostatic cancer treated by orchiectomy; the five year results. J. Am. Med. Assoc. *131*, 576–581.
5. Barrie, S.E., Potter, G.A., Goddard, P.M., Haynes, B.P., Dowsett, M., and Jarman, M. (1994). Pharmacology of novel steroidal inhibitors of cytochrome P450(17) alpha (17 alpha-hydroxylase/C17-20 lyase). J. Steroid Biochem. Mol. Biol. *50*, 267–273.
6. Watson, P.A., Arora, V.K., and Sawyers, C.L. (2015). Emerging mechanisms of resistance to androgen receptor inhibitors in prostate cancer. Nat. Rev. Cancer *15*, 701–711.
7. Beltran, H., Rickman, D.S., Park, K., Chae, S.S., Sboner, A., MacDonald, T.Y., Wang, Y., Sheikh, K.L., Terry, S., Tagawa, S.T., et al. (2011). Molecular characterization of neuroendocrine prostate cancer and identification of new drug targets. Cancer Discov. *1*, 487–495.
8. Aggarwal, R., Zhang, T., Small, E.J., and Armstrong, A.J. (2014). Neuroendocrine prostate cancer: subtypes, biology, and clinical outcomes. J. Natl. Compr. Cancer Netw. *12*, 719–726.

9. Antonarakis, E.S., Lu, C., Wang, H., Luber, B., Nakazawa, M., Roeser, J.C., Chen, Y., Mohammad, T.A., Chen, Y., Fedor, H.L., et al. (2014). AR-V7 and resistance to enzalutamide and abiraterone in prostate cancer. New Engl. J. Med. *371*, 1028–1038.

10. Chen, E.J., Sowalsky, A.G., Gao, S., Cai, C., Voznesensky, O., Schaefer, R., Loda, M., True, L.D., Ye, H., Troncoso, P., et al. (2015). Abiraterone treatment in castration-resistant prostate cancer selects for progesterone responsive mutant androgen receptors. Clin. Cancer Res. *21*, 1273–1280.

11. Zhao, X.Y., Malloy, P.J., Krishnan, A.V., Swami, S., Navone, N.M., Peehl, D.M., and Feldman, D. (2000). Glucocorticoids can promote androgen-independent growth of prostate cancer cells through a mutated androgen receptor. Nat. Med. *6*, 703–706.

12. Arora, V.K., Schenkein, E., Murali, R., Subudhi, S.K., Wongvipat, J., Balbas, M.D., Shah, N., Cai, L., Efstathiou, E., Logothetis, C., et al. (2013). Glucocorticoid receptor confers resistance to antiandrogens by bypassing androgen receptor blockade. Cell *155*, 1309–1322.

13. Veldscholte, J., Ris-Stalpers, C., Kuiper, G.G., Jenster, G., Berrevoets, C., Claassen, E., van Rooij, H.C., Trapman, J., Brinkmann, A.O., and Mulder, E. (1990). A mutation in the ligand binding domain of the androgen receptor of human LNCaP cells affects steroid binding characteristics and response to anti-androgens. Biochem. Biophys. Res. Commun. *173*, 534–540.

14. Li, J., Alyamani, M., Zhang, A., Chang, K.H., Berk, M., Li, Z., Zhu, Z., Petro, M., Magi-Galluzzi, C., Taplin, M.E., et al. (2017). Aberrant corticosteroid metabolism in tumor cells enables GR takeover in enzalutamide resistant prostate cancer. eLife *6*, e20183.

15. Yamashita, K., Kobayashi, S., Tsukamoto, S., and Numazawa, M. (2007a). Synthesis of pyridine-carboxylate derivatives of hydroxysteroids for liquid chromatography-electrospray ionization-mass spectrometry. Steroids *72*, 50–59.

16. Yamashita, K., Okuyama, M., Watanabe, Y., Honma, S., Kobayashi, S., and Numazawa, M. (2007b). Highly sensitive determination of estrone and estradiol in human serum by liquid chromatography-electrospray ionization tandem mass spectrometry. Steroids *72*, 819–827.

17. Pihlajamaa, P., Sahu, B., and Janne, O.A. (2015). Determinants of receptor- and tissue-specific actions in androgen signaling. Endocr. Rev. *36*, 357–384.

18. Paakinaho, V., and Palvimo, J.J. (2021). Genome-wide crosstalk between steroid receptors in breast and prostate cancers. Endocr. Relat. Cancer *28*, R231–R250.

19. Scher, H.I., Fizazi, K., Saad, F., Taplin, M.E., Sternberg, C.N., Miller, K., de Wit, R., Mulders, P., Chi, K.N., Shore, N.D., et al. (2012). Increased survival with enzalutamide in prostate cancer after chemotherapy. New Engl. J. Med. *367*, 1187–1197.

20. Tran, C., Ouk, S., Clegg, N.J., Chen, Y., Watson, P.A., Arora, V., Wongvipat, J., Smith-Jones, P.M., Yoo, D., Kwon, A., et al. (2009). Development of a second-generation antiandrogen for treatment of advanced prostate cancer. Science *324*, 787–790.

21. Borgmann, H., Lallous, N., Ozistanbullu, D., Beraldi, E., Paul, N., Dalal, K., Fazli, L., Haferkamp, A., Lejeune, P., Cherkasov, A., and Gleave, M.E. (2018). Moving towards precision urologic oncology: targeting enzalutamide-resistant prostate cancer and mutated forms of the androgen receptor using the novel inhibitor darolutamide (ODM-201). Eur. Urol. *73*, 4–8.

22. Hara, T., Miyazaki, J., Araki, H., Yamaoka, M., Kanzaki, N., Kusaka, M., and Miyamoto, M. (2003). Novel mutations of androgen receptor: a possible mechanism of bicalutamide withdrawal syndrome. Cancer Res. *63*, 149–153.

23. Liberzon, A., Birger, C., Thorvaldsdottir, H., Ghandi, M., Mesirov, J.P., and Tamayo, P. (2015). The Molecular Signatures Database (MSigDB) hallmark gene set collection. Cell Syst. *1*, 417–425.

24. Cuzick, J., Swanson, G.P., Fisher, G., Brothman, A.R., Berney, D.M., Reid, J.E., Mesher, D., Speights, V.O., Stankiewicz, E., Foster, C.S., et al. (2011). Prognostic value of an RNA expression signature derived from cell cycle proliferation genes in patients with prostate cancer: a retrospective study. Lancet Oncol. *12*, 245–255.

25. Penney, K.L., Sinnott, J.A., Fall, K., Pawitan, Y., Hoshida, Y., Kraft, P., Stark, J.R., Fiorentino, M., Perner, S., Finn, S., et al. (2011). mRNA expression signature of Gleason grade predicts lethal prostate cancer. J. Clin. Oncol. *29*, 2391–2396.

26. Kumar, A., Coleman, I., Morrissey, C., Zhang, X., True, L.D., Gulati, R., Etzioni, R., Bolouri, H., Montgomery, B., White, T., et al. (2016). Substantial interindividual and limited intraindividual genomic diversity among tumors from men with metastatic prostate cancer. Nat. Med. *22*, 369–378.

27. Tang, Z., Li, C., Kang, B., Gao, G., Li, C., and Zhang, Z. (2017). GEPIA: a web server for cancer and normal gene expression profiling and interactive analyses. Nucleic Acids Res. *45*, W98–W102.

28. Taylor, B.S., Schultz, N., Hieronymus, H., Gopalan, A., Xiao, Y., Carver, B.S., Arora, V.K., Kaushik, P., Cerami, E., Reva, B., et al. (2010). Integrative genomic profiling of human prostate cancer. Cancer Cell *18*, 11–22.

29. Cerami, E., Gao, J., Dogrusoz, U., Gross, B.E., Sumer, S.O., Aksoy, B.A., Jacobsen, A., Byrne, C.J., Heuer, M.L., Larsson, E., et al. (2012). The cBio cancer genomics portal: an open platform for exploring multidimensional cancer genomics data. Cancer Discov. *2*, 401–404.

30. Keenan, A.B., Torre, D., Lachmann, A., Leong, A.K., Wojciechowicz, M.L., Utti, V., Jagodnik, K.M., Kropiwnicki, E., Wang, Z., and Ma'ayan, A. (2019). ChEA3: transcription factor enrichment analysis by orthogonal omics integration. Nucleic Acids Res. *47*, W212–W224.

31. Umetani, M., Nakao, H., Doi, T., Iwasaki, A., Ohtaka, M., Nagoya, T., Mataki, C., Hamakubo, T., and Kodama, T. (2000). A novel cell adhesion inhibitor, K-7174, reduces the endothelial VCAM-1 induction by inflammatory cytokines, acting through the regulation of GATA. Biochem. Biophys. Res. Commun. *272*, 370–374.

32. Alyamani, M., Li, Z., Berk, M., Li, J., Tang, J., Upadhyay, S., Auchus, R.J., and Sharifi, N. (2017). Steroidogenic metabolism of galeterone reveals a diversity of biochemical activities. Cell Chem. Biol. *24*, 825–832.e6.

33. Li, Z., Alyamani, M., Li, J., Rogacki, K., Abazeed, M., Upadhyay, S.K., Balk, S.P., Taplin, M.E., Auchus, R.J., and Sharifi, N. (2016). Redirecting abiraterone metabolism to fine-tune prostate cancer anti-androgen therapy. Nature *533*, 547–551.

34. Han, Y., Zhuang, Q., Sun, B., Lv, W., Wang, S., Xiao, Q., Pang, B., Zhou, Y., Wang, F., Chi, P., et al. (2021). Crystal structure of steroid reductase SRD5A reveals conserved steroid reduction mechanism. Nat. Commun. *12*, 449.

35. Hou, Z., Yang, T., Mei, Z., Zhang, S., Gao, Y., Chen, X., Tan, Q., Zhu, X., Xu, C., Lian, J., et al. (2021b). Tracing steroidogenesis in prostate biopsy samples to unveil prostate tissue androgen metabolism characteristics and potential clinical application. J. Steroid Biochem. Mol. Biol. *210*, 105859.

36. Matias, P.M., Donner, P., Coelho, R., Thomaz, M., Peixoto, C., Macedo, S., Otto, N., Joschko, S., Scholz, P., Wegg, A., et al. (2000). Structural evidence for ligand specificity in the binding domain of the human androgen receptor. Implications for pathogenic gene mutations. J. Biol. Chem. *275*, 26164–26171.

37. Thomas, J.L., Bucholtz, K.M., and Kacsoh, B. (2011b). Selective inhibition of human 3beta-hydroxysteroid dehydrogenase type 1 as a potential treatment for breast cancer. J. Steroid Biochem. Mol. Biol. *125*, 57–65.

38. Labrie, F. (2015). Combined blockade of testicular and locally made androgens in prostate cancer: a highly significant medical progress based upon intracrinology. J. Steroid Biochem. Mol. Biol. *145*, 144–156.

39. Pernigoni, N., Zagato, E., Calcinotto, A., Troiani, M., Mestre, R.P., Cali, B., Attanasio, G., Troisi, J., Minini, M., Mosole, S., et al. (2021). Commensal bacteria promote endocrine resistance in prostate cancer through androgen biosynthesis. Science *374*, 216–224.

40. Li, J., Daly, E., Campioli, E., Wabitsch, M., and Papadopoulos, V. (2014). De novo synthesis of steroids and oxysterols in adipocytes. J. Biol. Chem. *289*, 747–764.

41. Pham, J.H., Will, C.M., Mack, V.L., Halbert, M., Conner, E.A., Bucholtz, K.M., and Thomas, J.L. (2017). Structure-function relationships for the selective inhibition of human 3beta-hydroxysteroid dehydrogenase type 1 by a novel androgen analog. J. Steroid Biochem. Mol. Biol. *174*, 257–264.

42. Chen, C.Y., Chen, C.C., Shieh, T.M., Hsueh, C., Wang, S.H., Leu, Y.L., Lian, J.H., and Wang, T.H. (2018). Corylin suppresses hepatocellular carcinoma progression via the inhibition of epithelial-mesenchymal transition, mediated by long noncoding RNA GAS5. Int. J. Mol. Sci. *19*, 380.

43. Zheng, Z.G., Zhang, X., Liu, X.X., Jin, X.X., Dai, L., Cheng, H.M., Jing, D., Thu, P.M., Zhang, M., Li, H., et al. (2019). Inhibition of HSP90beta improves lipid disorders by promoting mature SREBPs degradation via the ubiquitin-proteasome system. Theranostics *9*, 5769–5783.

44. Jafari, R., Almqvist, H., Axelsson, H., Ignatushchenko, M., Lundback, T., Nordlund, P., and Martinez Molina, D. (2014). The cellular thermal shift assay for evaluating drug target interactions in cells. Nat. Protoc. *9*, 2100–2122.

45. Matsubara, N., Chi, K.N., Ozguroglu, M., Rodriguez-Antolin, A., Feyerabend, S., Fein, L., Alekseev, B.Y., Sulur, G., Protheroe, A., Li, S., et al. (2020). Correlation of prostate-specific antigen kinetics with overall survival and radiological progression-free survival in metastatic castration-sensitive prostate cancer treated with abiraterone acetate plus prednisone or placebos added to androgen deprivation therapy: post hoc analysis of phase 3 LATITUDE study. Eur. Urol. *77*, 494–500.

46. Clarke, C.L., and Sutherland, R.L. (1990). Progestin regulation of cellular proliferation. Endocr. Rev. *11*, 266–301.

47. Ferretti, G., Felici, A., and Cognetti, F. (2007). The protective side of progesterone. Breast Cancer Res. *9*, 402.

48. Ishibashi, H., Suzuki, T., Suzuki, S., Niikawa, H., Lu, L., Miki, Y., Moriya, T., Hayashi, S., Handa, M., Kondo, T., and Sasano, H. (2005). Progesterone receptor in non-small cell lung cancer–a potent prognostic factor and possible target for endocrine therapy. Cancer Res. *65*, 6450–6458.

49. Slattery, M.L., Samowitz, W.S., and Holden, J.A. (2000). Estrogen and progesterone receptors in colon tumors. Am. J. Clin. Pathol. *113*, 364–368.

50. Cowan, L.D., Gordis, L., Tonascia, J.A., and Jones, G.S. (1981). Breast cancer incidence in women with a history of progesterone deficiency. Am. J. Epidemiol. *114*, 209–217.

51. Yu, Y., Liu, L., Xie, N., Xue, H., Fazli, L., Buttyan, R., Wang, Y., Gleave, M., and Dong, X. (2013). Expression and function of the progesterone receptor in human prostate stroma provide novel insights to cell proliferation control. J. Clin. Endocrinol. Metab. *98*, 2887–2896.

52. Kaore, S.N., Langade, D.K., Yadav, V.K., Sharma, P., Thawani, V.R., and Sharma, R. (2012). Novel actions of progesterone: what we know today and what will be the scenario in the future? J. Pharm. Pharmacol. *64*, 1040–1062.

53. Attard, G., Reid, A.H., Yap, T.A., Raynaud, F., Dowsett, M., Settatree, S., Barrett, M., Parker, C., Martins, V., Folkerd, E., et al. (2008). Phase I clinical trial of a selective inhibitor of CYP17, abiraterone acetate, confirms that castration-resistant prostate cancer commonly remains hormone driven. J. Clin. Oncol. *26*, 4563–4571.

54. McKay, R.R., Werner, L., Mostaghel, E.A., Lis, R., Voznesensky, O., Zhang, Z., Marck, B.T., Matsumoto, A.M., Domachevsky, L., Zukotynski, K.A., et al. (2017). A phase II trial of abiraterone combined with dutasteride for men with metastatic castration-resistant prostate cancer. Clin. Cancer Res. *23*, 935–945.

55. L Lallous, N., Volik, S.V., Awrey, S., Leblanc, E., Tse, R., Murillo, J., Singh, K., Azad, A.A., Wyatt, A.W., LeBihan, S., et al. (2016). Functional analysis of androgen receptor mutations that confer anti-androgen resistance identified in circulating cell-free DNA from prostate cancer patients. Genome Biol. *17*, 10.

56. Cai, C., Chen, S., Ng, P., Bubley, G.J., Nelson, P.S., Mostaghel, E.A., Marck, B., Matsumoto, A.M., Simon, N.I., Wang, H., et al. (2011). Intratumoral de novo steroid synthesis activates androgen receptor in castration-resistant prostate cancer and is upregulated by treatment with CYP17A1 inhibitors. Cancer Res. *71*, 6503–6513.

57. Ghashghaei, M., Niazi, T.M., Aguilar-Mahecha, A., Klein, K.O., Greenwood, C.M.T., Basik, M., and Muanza, T.M. (2019). Identification of a radiosensitivity molecular signature induced by enzalutamide in hormone-sensitive and hormone-resistant prostate cancer cells. Scientific Rep. *9*, 8838.

58. Alumkal, J.J., Sun, D., Lu, E., Beer, T.M., Thomas, G.V., Latour, E., Aggarwal, R., Cetnar, J., Ryan, C.J., Tabatabaei, S., et al. (2020). Transcriptional profiling identifies an androgen receptor activity-low, stemness program associated with enzalutamide resistance. Proc. Natl. Acad. Sci. U S A. *117*, 12315–12323.

59. Yasumizu, Y., Rajabi, H., Jin, C., Hata, T., Pitroda, S., Long, M.D., Hagiwara, M., Li, W., Hu, Q., Liu, S., et al. (2020). MUC1-C regulates lineage plasticity driving progression to neuroendocrine prostate cancer. Nat. Commun. *11*, 338.

60. Nordin, A., Wang, W., Welen, K., and Damber, J.E. (2013). Midkine is associated with neuroendocrine differentiation in castration-resistant prostate cancer. Prostate *73*, 657–667.

61. Hagiwara, M., Yasumizu, Y., Yamashita, N., Rajabi, H., Fushimi, A., Long, M.D., Li, W., Bhattacharya, A., Ahmad, R., Oya, M., et al. (2021). MUC1-C activates the BAF (mSWI/SNF) complex in prostate cancer stem cells. Cancer Res. *81*, 1111–1122.

62. Broustas, C.G., Hopkins, K.M., Panigrahi, S.K., Wang, L., Virk, R.K., and Lieberman, H.B. (2019). RAD9A promotes metastatic phenotypes through transcriptional regulation of anterior gradient 2 (AGR2). Carcinogenesis *40*, 164–172.

63. He, B., Lanz, R.B., Fiskus, W., Geng, C., Yi, P., Hartig, S.M., Rajapakshe, K., Shou, J., Wei, L., Shah, S.S., et al. (2014). GATA2 facilitates steroid receptor coactivator recruitment to the androgen receptor complex. Proc. Natl. Acad. Sci. U S A. *111*, 18261–18266.

64. Chaytor, L., Simcock, M., Nakjang, S., Heath, R., Walker, L., Robson, C., Jones, D., and Gaughan, L. (2019). The pioneering role of GATA2 in androgen receptor variant regulation is controlled by bromodomain and extraterminal proteins in castrate-resistant prostate cancer. Mol. Cancer Res. *17*, 1264–1278.

65. Rodriguez-Bravo, V., Carceles-Cordon, M., Hoshida, Y., Cordon-Cardo, C., Galsky, M.D., and Domingo-Domenech, J. (2017). The role of GATA2 in lethal prostate cancer aggressiveness. Nat. Rev. Urol. *14*, 38–48.

66. Robinson, J.L., Tzou, K.S., Parker, A.S., Heckman, M.G., Wu, K.J., Hilton, T.W., Pisansky, T.M., Schild, S.E., Peterson, J.L., Vallow, L.A., and Buskirk, S.J. (2017). GATA2 expression and biochemical recurrence following salvage radiation therapy for relapsing prostate cancer. Br. J. Radiol. *90*, 20170174.

67. Li, Z., Bishop, A.C., Alyamani, M., Garcia, J.A., Dreicer, R., Bunch, D., Liu, J., Upadhyay, S.K., Auchus, R.J., and Sharifi, N. (2015). Conversion of abiraterone to D4A drives anti-tumour activity in prostate cancer. Nature *523*, 347–351.

68. Roychowdhury, S., and Chinnaiyan, A.M. (2013). Advancing precision medicine for prostate cancer through genomics. J. Clin. Oncol. *31*, 1866–1873.

69. Khalaf, D.J., Aragon, I.M., Annala, M., Lozano, R., Taavitsainen, S., Lorente, D., Finch, D.L., Romero-Laorden, N., Vergidis, J., Cendon, Y., et al. (2020). HSD3B1 (1245A>C) germline variant and clinical outcomes in metastatic castration-resistant prostate cancer patients treated with abiraterone and enzalutamide: results from two prospective studies. Ann. Oncol. *31*, 1186–1197.

70. Lu, C., Terbuch, A., Dolling, D., Yu, J., Wang, H., Chen, Y., Fountain, J., Bertan, C., Sharp, A., Carreira, S., et al. (2020). Treatment with abiraterone and enzalutamide does not overcome poor outcome from metastatic

castration-resistant prostate cancer in men with the germline homozygous HSD3B1 c.1245C genotype. Ann. Oncol. *31*, 1178–1185.

71. Scher, H.I., Halabi, S., Tannock, I., Morris, M., Sternberg, C.N., Carducci, M.A., Eisenberger, M.A., Higano, C., Bubley, G.J., Dreicer, R., et al. (2008). Design and end points of clinical trials for patients with progressive prostate cancer and castrate levels of testosterone: recommendations of the Prostate Cancer Clinical Trials Working Group. J. Clin. Oncol. *26*, 1148–1159.

72. L Lee, S.H., Lee, N., Hong, Y., Chung, B.C., and Choi, M.H. (2016). Simultaneous analysis of free and sulfated steroids by liquid chromatography/mass spectrometry with selective mass spectrometric scan modes and polarity switching. Anal. Chem. *88*, 11624–11630.

73. Drost, J., Karthaus, W.R., Gao, D., Driehuis, E., Sawyers, C.L., Chen, Y., and Clevers, H. (2016). Organoid culture systems for prostate epithelial and cancer tissue. Nat. Protoc. *11*, 347–358.

74. Han, Y., Huang, W., Liu, J., Liu, D., Cui, Y., Huang, R., Yan, J., and Lei, M. (2017). Triptolide inhibits the AR signaling pathway to suppress the proliferation of enzalutamide resistant prostate cancer cells. Theranostics *7*, 1914–1927.

STAR★METHODS

KEY RESOURCES TABLE

REAGENT or RESOURCE	SOURCE	IDENTIFIER
Antibodies		
Anti-AR	Santa Cruz Biotechnology	Cat#sc-7305; RRID: AB_626671
Anti-GATA2	R&D Systems	Cat#AF2046; RRID: AB_355123
Anti-ACTB	ABClonal	Cat#AC004; RRID: AB_2737399
Anti-ERα (D8H8)	Cell Signaling Technology	Cat#8644; RRID: AB_2617128
Anti-Mouse IgG (H + L)	Jackson ImmunoResearch Labs	Cat#115-035-003; RRID: AB_10015289
Anti-Rabbit IgG (H+L)	Jackson ImmunoResearch Labs	Cat#111-035-003; RRID: AB_2313567
anti-Goat IgG-HRP	Absin Bioscience	Cat#abs20005; RRID: AB_2832210
Anti-AR (D6F11)	Cell Signaling Technology	Cat#5153; RRID: AB_10691711
anti-Rabbit IgG (H+L) Secondary Antibody	Thermo Fisher Scientific	Cat#A-11035; RRID: AB_2534093
Bacterial and Virus Strains		
DH5α	TIANGEN Biotch	Cat#CB101
Biological Samples		
Patient plasma	Tongji Hospital (Shanghai)	Table S1-S3
Patient biopsies	Tongji Hospital (Shanghai)	Hou et al.[35]
Chemicals, Peptides, and Recombinant Proteins		
RPMI-1640 Medium, with L-glutamine and sodium bicarbonate	Sigma-Aldrich	Cat#R8758
RPMI-1640 Medium, without L-glutamine and phenol red	Sigma-Aldrich	Cat#R7509
DMEM - high glucose	Sigma-Aldrich	Cat#D7777
DMEM, without glucose, L-glutamine, phenol red, sodium pyruvate and sodium bicarbonate	Sigma-Aldrich	Cat#D5030
IMDM	Sigma-Aldrich	Cat#I3390
IMDM, without Gentamicin Sulfate and phenol red	Sigma-Aldrich	Cat#A10488
Trypsin-EDTA solution	Sigma-Aldrich	Cat#T4049
Fetal Bovine Serum	Lonsera	Cat#S711-001S
Charcoal stripped FBS	Lonsera	Cat#S883811
L-Glutamine solution	Sigma-Aldrich	Cat#G7513
Sodium pyruvate	Sigma-Aldrich	Cat#11360070
Lipofectamine 3000	Invitrogen	Cat#L3000-015
Lipofectamine RNAiMAX	Invitrogen	Cat#13778150
Puromycin	GIBCO	Cat#A1113802
G418, Geneticin	GIBCO	Cat#10131035
Pregnenolone	Steraloids Inc.	Cat#Q5500-000
Progesterone	Steraloids Inc.	Cat#Q2600-000
5α-progesterone	Steraloids Inc.	Cas#566-65-4
3α-OH-5α-progesterone	Steraloids Inc.	Cas#516-54-1
3β-OH-5α-progesterone	Steraloids Inc.	Cas#516-55-2
5β-progesterone	Steraloids Inc.	Cas#128-23-4
3α-OH-5β-progesterone	Steraloids Inc.	Cas#128-20-1
3β-OH-5β-progesterone	Steraloids Inc.	Cas#128-21-2
Doxycycline hyclate	Sigma-Aldrich	Cat#10592-13-9
Polyethylenimine	Sigma-Aldrich	Cat#408727

(*Continued on next page*)

Continued

REAGENT or RESOURCE	SOURCE	IDENTIFIER
Biochanin A (BCA)	MedChem Express	Cat#HY-14595
K7174	MedChem Express	Cat#HY-12743A
Dihydrotestosterone (DHT)	MedChem Express	Cas#521-18-6
Dehydroepiandrosterone (DHEA)	Steraloids	Cat#A8500-000; Cas#3-43-0
Enzalutamide (MDV3100)	Foreversyn	Cas#915087-33-1
Protease inhibitor cocktails	MedChem Express	Cat#HY-K0011
Poly-DL-ornithine	Sigma-Aldrich	Cat#P3655-1G
Progesterone pellets	EZBioscience	N/A
Pregnenolone pellets	EZBioscience	N/A
Ethyl alcohol	Thermo Fisher Scientific	Cat#AC 615095000
Corn oil	ABCONE	Cat#C67366
Corning® Matrigel® Basement Membrane Matrix, *LDEV-Free	BD biocoat (Corning)	Cat#354234
[^{3}H]-DHEA	PerkinElmer	NET 814001MC
[^{3}H]-AD	PerkinElmer	NET 926005MC
[^{3}H]-Pregnenolone	PerkinElmer	NET 039001MC
[^{3}H]-R1881	PerkinElmer	NET 590250VC
[^{3}H]-Progesterone	PerkinElmer	NET 381
Methanol	Thermo Fisher Scientific	Cat#A454K4
Ethyl acetate	Sigma-Aldrich	Cat#34858-4L
Iso octane	Thermo Fisher Scientific	Cat#03014
Liquiscint scintillation cocktail	Thermo Fisher Scientific	Cat#5089990170
Tert-butyl methyl ether	Thermo Fisher Scientific	Cat#AC 389050025
TRIzol reagent	Thermo Fisher Scientific	Cat#15596026
Critical Commercial Assays		
Cell Counting Kit-8	Beyotime	Cat#C0038
Cell to cDNA Kit	EZBioscience	Cat#B0003
2x SYBR Green qPCR master mix	EZBioscience	Cat#A0001-R2
Pierce BCA Protein Assay Kit	Thermal Fisher Scientific	Cat#23225
Pierce ECL Western Blotting Substrate	Thermal Fisher Scientific	Cat#32209
KOD Hot Start DNA Polymerase	Novagen	Cat#71086-3
Glo Lysis Buffer, 1X	Promega	Cat#E266A
Bright-Glo™ Luciferase Assay System	Promega	Cat#E2160
VAHTS™ mRNA-seq V3 Library Prep Kit for Illumina	Vazyme	Cat#NR611
VAHTS™ RNA Adapters set3 - set6 for Illumina	Vazyme	Cat#N809/N810/N811/N812
Deposited Data		
Raw sequencing data	This paper	OEP002363; OEP002519
Plasma metabolites	This paper	OED660544; OED660545; OED660546
Experimental Models: Cell Lines		
LNCaP	ATCC	CRL-1740
VCaP	Dr. Jun Qin (SINH, China)	N/A
C4-2	ATCC	CRL-3314
LAPC4	Dr. Charles Sawyers (MSKCC, USA)	N/A
PC3	ATCC	CRL-1435
DU145	ATCC	HTB-81
HEK293T	ATCC	CRL-3216
HEK293	ATCC	CRL-1573
PC3-AR^{mut}	This paper	N/A

(*Continued on next page*)

Continued

REAGENT or RESOURCE	SOURCE	IDENTIFIER
LAPC4-AR^{mut}	This paper	N/A
VCaP-HSD3B1	This paper	N/A
Ctrl_cells	This paper	N/A
Prog_cells	This paper	N/A
Experimental Models: Organisms/Strains		
Mouse: NOD/SCID	Shanghai Lingchang Biotechnology	N/A
Mouse:*Pb*$^{Cre/+}$; *Pten*$^{flox/flox}$ (C57BL/6 background)	Dr. Jun Qin (SINH, China)	N/A
Oligonucleotides		
Primers used for real-time quantitative PCR and RT-PCR	This paper	Table S6
siRNA used for knocking down gene expression	This paper	Table S7
Recombinant DNA		
pLVX-Tight-Puro (TetOn)	Clonetech	Cat#632162
pGL3-PSA-Luc reporter plasmid	Dr. Jun Yan (Fudan University, China)	N/A
Software and Algorithms		
GraphPad Prism v8.0	GraphPad Software Inc	https://www.graphpad.com/scientific-software/prism
FastQC v0.11.7	Babraham Bioinformatics Institute	https://www.bioinformatics.babraham.ac.uk/projects/fastqc/
R v3.4.1	R Core Team	https://www.r-project.org/
R Studio	RStudio Team	https://www.rstudio.com/
pheatmap	R Core Team	https://cran.r-project.org/web/ packages/pheatmap/index.html
survival	R Core Team	https://cran.r-project.org/web/packages/survival/index.html
survminer	R Core Team	https://cran.r-project.org/web/packages/survminer/index.html
ggplot2	R Core Team	https://cran.r-project.org/web/packages/ggplot2/index.html
ChEA3	Keenan et al.[30]	https://maayanlab.cloud/chea3/
PyMOL	The PyMOL Molecular Graphics System, Version 2.0 Schrödinger, LLC.	https://pymol.org/2/
Data Availability		
RNA-seq raw data	This paper	OEP 002363 (https://www.biosino.org/node/project/detail/OEP002363) and OEP 002519 (https://www.biosino.org/node/project/detail/OEP002519).
Metabonomics data	This paper	OED660544 (https://www.biosino.org/download/node/data/OED660544), OED660545 (https://www.biosino.org/download/node/data/OED660545), OED660546 (https://www.biosino.org/download/node/data/OED660546)
Published datasets	cBioPortal database	http://www.cbioportal.org

RESOURCE AVAILABILITY

Lead contact

Further information and request for resources and reagents should be directed to and will be fulfilled by the Lead Contact, Dr. Zhenfei Li (zhenfei.li@sibcb.ac.cn).

Materials availability

The plasmids, antibodies, stable cell lines and chemical compounds generated in this study have not been deposited to any repositories yet, however, these materials would be available from the Lead Contact without restriction.

Data and code availability

All RNA-seq data generated during this study have been deposited in the National Omics Data Encyclopedia/NODE (https://www.biosino.org/node) under the accession number OEP 002363 (https://www.biosino.org/node/project/detail/OEP002363) and OEP 002519 (https://www.biosino.org/node/project/detail/OEP002519). Metabolites detected in Figure 1A were also deposited in NODE with accession number OED660544 (https://www.biosino.org/download/node/data/OED660544), OED660545 (https://www.biosino.org/download/node/data/OED660545), OED660546 (https://www.biosino.org/download/node/data/OED660546). Published datasets used in this study are available through cBioPortal database (http://www.cbioportal.org). This paper does not report original code. Any additional information required to reanalyze the data reported in this work paper is available from the Lead Contact upon request.

EXPERIMENTAL MODEL AND SUBJECT DETAILS

Patients

All investigations in this study were conducted according to the principles of the Declaration of Helsinki. All patient studies were performed according to the relevant ethical standards and were approved by the Ethics Committee of Tongji Hospital, Shanghai, China (ID: 2018009). Written consents from all patients were obtained. Clinical information of the patients receiving abiraterone acetate treatment at the Shanghai Tongji Hospital between August 2016 and April 2020 were analyzed. A total of 103 patients received abiraterone treatment and 90 patients with endocrine hormone related examination and regular follow-up were qualified for further analysis. The castrate-level of testosterone was also confirmed in these patients. Endocrine hormone-related laboratory indices were determined by clinical laboratory and the 16 indexes includes luteinizing hormone (LH), follicle-stimulating hormone (FSH), pituitary prolactin, neuron-specific enolase (NSE), alanine aminotransferase (ALT), aspartate aminotransferase (AST), sex hormone-binding globulin (SHBG), total cholesterol (TC), triglyceride (TG), dehydroepiandrosterone (DHEA), androstenedione (AD), testosterone (T), free testosterone (FT), dihydrotestosterone (DHT), progesterone, and estradiol (E2). Paired Student's t test and false discovery rate (FDR) were used to compare the differences between the baseline and endpoint of abiraterone treatment. Threshold criteria for all differential-expression analyses are an absolute value ($\log_2$ (fold-change)) $\geq$ 1 and FDR $<$ 0.05. Among these 90 patients, 73 patients had the information of plasma progesterone levels at baseline or after abiraterone treatment. PSA progression was determined according to the PCWG2 guidelines.[71]

Cell lines

LNCaP, HEK293, HEK293T, PC3, DU145 cells were purchased from the American Type Culture Collection (Manassas, VA, USA) and cultured in RPMI-1640 (LNCaP, PC3, DU145) or DMEM (HEK 293, HEK293T) with 10% or 5% (PC3) FBS (Lonsera, China). LAPC4 cells were grown in Iscove's modified Dulbecco's medium with 10% FBS and 1% L-glutamine (final c.c 2 mM; Gibco, Life Technologies). VCaP was kindly provided by Dr. Jun Qin (SINH, Shanghai, China), and cultured in DMEM with 10% or 5% (PC3) FBS and 1% Sodium Pyruvate (final c.c 1 mM; Gibco, Life Technologies). Stable PC3 and LAPC4 cell lines with AR and 3βHSD1 overexpression were established using lentiviral plasmids pLVX-tight-puro and pLVX-tet-on. LAPC4 cells were cultured with ethanol or 5 nM progesterone for 6 months to establish Ctrl_cells and Prog_cells. All experiments with LNCaP, VCaP, and LAPC4 were performed in plates coated with poly-DL-ornithine (Sigma-Aldrich, St. Louis, MO, USA). All cell lines were authenticated by Hybribio (Guangzhou, China).

Animal models

All mice were maintained in a specific-pathogen-free (SPF) facility, and all related protocols were performed in compliance with the Guide for the Care and Use of Laboratory Animals and were approved by the Institutional Animal Care and Use Committee of Shanghai Institute of Biochemistry and Cell Biology, Chinese Academy of Sciences. Male NOD-SCID mice (aged 6 to 8 weeks) were obtained from Lingchang Biotech (Shanghai, China).

METHOD DETAILS

Reagents

2-picolinic acid (PA) and 2-methyl-6-nitrobenzonic anhydride (MNBA) were purchased from Aladdin (Shanghai, China), whereas 4-dimethylaminopyridine (DMPA) and anhydrous pyridine were obtained from J&K Scientific (Shanghai, China). All sterol standards examined in this study were purchased from J&K Scientific (Shanghai, China), Sigma-Aldrich (St Louis, MO, USA), Aladdin (Shanghai, China) and TRC (Toronto, Canada) as appropriate. Cholesterol-d7, campesterol-d3, estrone-d2, dehydroepiandrosterone-d2, estradiol-d2, 24-hydroxycholesterol-d7, and β-Sitosterol-d7 were purchased from Sigma-Aldrich (St Louis, MO, USA), CDN ISOTOPES

(Quebec, Canada) and CIL (Tewksbury, MA, USA) as appropriate. LC-grade acetonitrile and tert-butyl methyl ether were purchased from Sigma-Aldrich (St Louis, MO, USA), and pure water was obtained from a Milli-Q system (Merck Millipore, Germany).

Preparation of standard solutions for calibration curves

Stock solutions of all steroid standards were prepared at a concentration of approximately 1 mg/mL in methanol-dichloromethane (1:2 v/v); A set of standard solutions with concentrations of 0.003-390.6 μM were obtained by mixing the appropriate amounts of the above stock solutions. These working solutions were then stored at −20°C, which were found to remain stable for 6 months, until further analysis.

Preparation of plasma samples

Each plasma sample (50 μL) was added to 50 μL of an internal standard mixture consisting of cholesterol-d7, campesterol-d3, estrone-d2, dehydroepiandrosterone-d2, estradiol-d2, 24-Hydroxycholesterol-d7, and β-Sitosterol-d7. Then, 500 μL of pre-cooled methanol (−20°C) was added, vortexed, and centrifuged at 12000 rpm at 4°C for 10 min to obtain the supernatant. This extraction procedure was repeated once more and the two supernatants from each sample were pooled and dried using nitrogen gas. The residue was re-dissolved in 50 μL of acetonitrile. Five microliters of this solution was used directly to quantify steroids without hydroxyl groups, while the remaining solution was dried with nitrogen gas followed by derivatization to identify the sterols carrying the hydroxyl groups.

Derivatization of sterol metabolites with 2-Picolinic acid

Derivatization of sterol metabolites was conducted as reported previously[15,16] with some modifications. In brief, the nitrogen-dried residue of the working solution (10 μL) and biological sample extracts were added to 100 μL pyridine solution of PA, MNBA, and DMPA, respectively. The mixtures were heated at 80°C for 60 min, followed by the addition of pure water (200 μL) and extraction with MTBE (1.5 mL). These MTBE extracts were dried with nitrogen gas and the resultant residues were reconstituted in 100 μL acetonitrile for UHPLC- MS/MS analysis.

UHPLC-MS/MS analysis

Quantification was performed on an LC-30AD UHPLC system (Shimadzu Technologies, Japan) hyphenated with a 6500 plus Qtrap mass spectrometer (AB Sciex Corp., USA) with an electrospray ionization (ESI) source. A Zorbax Eclipse Plus C18 column (100 × 2.1 mm, 1.8 μm; Agilent, USA) was used with water and acetonitrile containing 0.1% formic acid as mobile phases A and B, respectively. The injection volume was 5 μL in all the cases. The ESI source parameters were as follows: ion spray voltage, 5500 V; curtain gas, 40 psi; temperature, 550°C; ion source gas 1.55 psi; ion source gas 2, 60 psi; entrance potential voltage, 10 V; collision cell exit potential, 10 V. Data were acquired and processed using Sciex software Analyst (V1.7) and OS (V2.0). The quantification of these steroids as their PA derivatives was achieved against their corresponding internal standards with known concentrations. The method was validated by assessing the linearity, limits of detection (LOD), and quantification (LOQ) at a signal-to-noise ratio of 10. Such approach offered useful mass spectral fragment ions and achieved excellent quantitation sensitivities with the low limit of quantification (LLOQ at signal-to-noise ratio of 10:1) reaching 10^{-15} mol on column. This method also simultaneously covered these steroids carrying no hydroxyl groups as they were with LLOQ of about 10^{-14} mol on column.[72] To the best of our knowledge, such quantitative sensitivity is well above what have reported so far.

Untargeted metabonomics analysis with UPLC-QTOFMS

Plasma samples were respectively extracted with cold methanol with final the methanol: water ratio of 5:1 (v/v) by vortex-mixing (45 s) followed with 10 min centrifugation (14,000 g, 4°C). The resultant supernatant was added with precooled water and MTBE with the final water: methanol: MTBE ratio of 5:6:20 (v/v) followed with 60 s mixing and 5 min centrifugation (14,000 g, 4°C). The lower layer was transferred into sample vials for LC-MS analysis. UPLC-QTOFMS analysis was conducted on a system consisting of a Waters ACQUITY UPLC and Xevo G2-XS QTOF mass spectrometry with an electrospray ionization (ESI) source (Waters, Milford, USA) equipped with a Waters ACQUITY UPLC HSS T3 column (2.1 × 100 mm, 1.8 μm). Water and acetonitrile (LC grade, Fisher Scientific, USA) both containing 0.1% formic acid (LC grade, Fisher Scientific, USA) were employed as the mobile phase A and B, respectively. The flow rate was 0.5 mL/min; injection volume was 1 μL and the column temperature was 40°C. Elution was performed with an optimized gradient condition as follows: 0-1 min, 1% B; 1-3 min, 1-15% B; 3-6 min, 15-50% B; 6-9 min, 50-95% B; 9-10 min, 95% B. The mass spectrometry data was acquired in both positive and negative ion modes as MSE Centroid format. The spectrometer parameters were as follows: capillary voltage 2.5 kV; cone voltage 30 V; ion source temperature 120°C; desolvation gas temperature 500°C; cone gas flow 50 L/h; desolvation gas flow 800 L/h; collision voltage range 10∼50 V; scan time 0.1 sec; mass range 50∼1000 Da; low CE 4 eV; and high CE 10∼50 eV. Lockspray was used for real-time acquisition and correction with the internal calibrator as leucine-enkephalin ($[M + H]^+$ = 556.2771, $[M - H]^-$ = 554.2615). Acquired data were imported into Progenesis QI software package to generate a list of peaks containing the mass-to-charge ratio (m/z), retention time (RT), and peak intensity. After removal of variables with RSD > 30%, such data were then subjected to QC-based corrections and normalization followed with statistical analysis and metabolite identification with in-house developed and publicly accessible databases (METLIN, HMDB, LipidBlast and Elemental composition). The results of the untargeted metabonomics analysis and targeted sterol quantification

were analyzed together or separately. Paired Student's t test and false discovery rate (FDR) were used to compare the differences between baseline and endpoint of abiraterone treatment. Threshold criteria for all differential-expression analyses are an absolute value (log_2 (fold-change)) $\geq$ 3 and FDR < 0.25. Common different metabolites found through metabolite screening and hormone screening in clinic were defined as potential cancer-associated metabolites.

Detection of plasma progesterone and its metabolites

For the detection of plasma progesterone and its metabolites, the extract of plasma samples was analyzed using a high-performance liquid chromatography station (Agilent, Santa Clara, CA) equipped with G4204A pumps, a G1367E auto-sampler, a G1316A column oven and a triple quadrupole 6490 (Agilent, Santa Clara, CA). The separation of drug metabolites was achieved using an Eclipse Plus C18 RRHD analytical column (3.0 mm × 50 mm, 1.8 μM; Agilent, Santa Clara, CA, USA) at 40°C with an isocratic mobile phase consisting of 10% buffer A (0.1% formic acid in methanol: water, 60:40) and 90% buffer B (0.1% formic acid in acetonitrile: water, 60:40), at a flow rate of 0.2 ml/min. The injection volume was 10 μL and sample injection was performed using an auto-sampler. All progesterone metabolites were ionized using electrospray ionization in the positive ion mode (ESI). The temperature of the drying gas in the ionization source was maintained at 225°C. The gas flow was 12 l/min, the nebulizer pressure was 35 psi, and the capillary voltage was 4000 V (positive) and 3000 V (negative). The analytes were quantified using multiple reaction monitoring with mass transitions and the parameters for each compound. Methanol and water were of LC–MS grade and all reagents were obtained from Thermo Fisher Scientific.

Chemical compounds

Pregnenolone, progesterone, 5α-progesterone, 3α-OH-5α-progesterone, 3β-OH-5α-progesterone, 5β-progesterone, 3α-OH-5β-progesterone, and 3β-OH-5β-progesterone were purchased from Steraloids Inc. (Newport, RI, USA). R1881 was purchased from Meilunbio Company (Dalian, China). DHT, BCA and K7174 were purchased from MCE (Shanghai Haoyuan Chemexpress, China). Doxycycline hyclate was purchased from Sigma-Aldrich (St. Louis, MO, USA). Tritium labelled androgens (R1881, pregnenolone, progesterone, dehydroepiandrosterone, or androstenedione) were purchased from PerkinElmer (Waltham, MA, USA).

Steroidogenesis in patient biopsy samples

2-3 mg biopsy samples were minced and cultured with DMEM (Invitrogen, Waltham, MA), 10% FBS (ExCell Bio, China), and Penicillin-Streptomycin (100 x; Invitrogen, Waltham, MA, USA) in a 12-well plate at 37°C as previously described.[35] Biopsy samples were treated with [^{3}H] labelled pregnenolone (100, 000–200,000 cpm; final concentration was 48 nM) (PerkinElmer, Waltham, MA, USA). 250 μl medium was collected at 84 h for HPLC analysis. Then, samples were treated with β-glucuronidase (Novoprotein Scientific Inc., Shanghai, China) at 37°C for 2 h. Steroids were extracted with a mixture of ethyl acetate and isooctane (1:1), concentrated with a vacuum drier (Martin Christ Gefriertrocknungsanlagen, Osterode, Germany), and resuspended with a mixture of methanol and water (1:1). An Acquity Arc System (Waters, Milford, MA, USA) and a β-RAM model 5 in-line radioactivity detector (LabLogic Systems) were used to analyze metabolites in samples. A mixture of [^{3}H] labelled androgens (AD, DHEA, Prog, Preg PerkinElmer, Waltham, MA, USA) was used as the standard to distinguish metabolites. The percentages of metabolites were calculated based on the area under curve (AUC) for each metabolite. For example, Preg % = (AUC of Preg)/ (AUC of Preg + AUC of all Preg metabolites) x 100 %.

Mouse prostatic organoids

Mouse prostatic organoids were generated as described previously.[73] In brief, the prostate gland from *Pb*$^{Cre/+}$; *Pten*$^{flox/flox}$ mice (12 week, male) were minced and digested in collagenase type II (5 mg/ml, Life Technologies) with 10 mM Y-27632 (#17101-015, Life Technologies). The dissociated tissues were further digested with TrypLE^{TM} Express (Gibco, Life Technologies), filtered with a 40 μm filter, and then stained with CD24-FITC (1:200, Biolegend) and PE conjugated CD49f (1:200, eBioscience). Cell sorting was performed using FACS Aria II (BD). For the organoid formation assay, the sorted mouse prostate cells were suspended and mixed with Matrigel (v/v 1:1). 2,000 cells were seeded into a 24-well plate, and organoid medium was added on top of the Matrigel. DHT was replaced with ethanol, progesterone, or pregnenolone in the culture medium and changed every 4 days. The number and size of the organoids were determined after one-week of culture.

HPLC

Steroid metabolism and HPLC were performed as described previously.[35] Briefly, cells or organoids were treated with [^{3}H]-labeled steroids (pregnenolone, DHEA, AD; 100,000-200,000 cpm per well; PerkinElmer, Waltham, MA). Aliquots of the medium were treated with β-glucuronidase (Novoprotein Scientific Inc., Shanghai, China) and extracted using a mixture of ethyl acetate and isooctane (1:1). Steroids were analyzed using an Acquity Arc System (Waters, Milford, MA, USA) and a β-RAM model 3 in-line radioactivity detector (LABLOGIC, USA). The percentages of metabolites were calculated based on the area under curve (AUC) for each metabolite. For example, pregnenolone% = (AUC of pregnenolone) / (AUC of pregnenolone + AUC of all metabolites) x 100 %.

Effects of periprostatic adipose tissue medium

Periprostatic adipose tissues were collected from prostate cancer patients receiving radical prostatectomy. Fresh adipose tissue of 60 mg was culture in 6 ml DMEM+10% FBS for two days and 100 μl medium was used to treat LNCaP cells for target gene assay. Pregnenolone was detected with LC-MS.

Gene expression

Generally, prostate cancer cells were starved for 48 h with phenol red-free medium and 5% heat-inactivated charcoal stripped FBS (CSS) (ExCell Bio, China) before treated with progesterone or other drugs. The Cell to cDNA Kit (EZBioscience, China) was used to synthesize cDNA directly from the cells according to the manufacturer's instructions. Real-time quantitative PCR (qPCR) was conducted using the CFX96 system (Bio-Rad, Hercules, CA, USA), using 2× SYBR Green qPCR master mix (EZBioscience, China). Results were presented as the mean and standard deviation (SD) from one representative experiment.

Cell proliferation assay

Prostate cancer cells were starved for 48 h with phenol red-free medium and 5% heat-inactivated charcoal stripped FBS (CSS) (ExCell Bio, China) for cell proliferation assay. Cell proliferation assay was performed using the cell counting kit-8 (#C0038, Beyotime, China) according to the manufacturer's instructions. 10,000 cells per well were seeded in a 96-well plate and starved with 5% heat-inactivated CSS (ExCell Bio, China) for 48 h. To count the viable cells, the absorbance was measured at 450 nm and 600 nm, using a microplate reader (BioTeK, Winooski, VT, US). Lipofectamine^{TM} RNAiMAX Transfection Reagent (Invitrogen, Waltham, MA, USA) was used for siRNA transfection (GenePharma Co. Ltd, Shanghai, China). Results were presented as the mean and SD values from one representative experiment.

Immunoblotting

Total protein was extracted from cells using RIPA buffer containing Pierce^{TM} protease inhibitors (Thermo Fisher Scientific). Total protein was quantified with Pierce^{TM} BCA Protein Assay (Thermo Fisher Scientific). The primary antibodies used were as follows: anti-AR (#sc-7305, 1:1,000, Santa Cruz), anti-GATA2 (#ab37917, 1:1,000, R&D), anti-β-actin (#AC038, 1:10,000, ABclonal), and anti-ESR1 (#8644, 1:1000, CST). The HRP-conjugated secondary antibodies were goat anti-mouse (#115-035-003, JACKSON), goat anti-rabbit (#111-035-003, JACKSON), rabbit anti-goat (#abs20005, absin).

Immunofluorescence

A total of 100,000 cells were seeded in a glass bottom cell culture dish (#801001, Nest) and starved for 24 h (VCaP) or 48 h (LNCaP). Cells were treated with ethanol, progesterone, and DHT for the indicated times. Cells were fixed and incubated with anti-AR antibody (#5153, 1:1000, Cell Signaling Technology) and goat anti-rabbit secondary antibody (#a11035, 1:500, Invitrogen) before analysis with fluorescence microscopy (Zeiss LSM 880 Fast Airyscan Confocal).

AR competition assay

Approximately 200,000 cells were seeded in 24-well plate and starved with phenol red-free medium and 5% CSS for 48 h. Cells were treated with 1 nM [^{3}H]-R1881 and other steroids at the indicated concentrations for 30 min. Intracellular radioactivity was measured using a Tri-Carb® 5110TR Low Activity Liquid Scintillation Analyzer (PerkinElmer, Waltham, MA, USA) and protein concentration was detected by a microplate reader (BioTeK, Winooski, VT, US) at an absorbance of 562 nm.

Luciferase reporter gene assay

The PSA-luciferase reporter was kindly provided by Dr. Jun Yan (Fudan University, Shanghai, China) and transfected together with a plasmid expressing GFP into HEK 293T cells. Cells were treated with R1881 or progesterone for 24 h. Luciferase activity and GFP intensity in cell lysates were determined as described previously.[74]

Mouse xenograft studies

All mouse studies were conducted under a protocol approved by the Institutional Animal Care and Use Committee. Male NOD-SCID mice (aged 6 to 8 weeks) were obtained from Lingchang Biotech (Shanghai, China) and kept in a specific pathogen free (SPF) facility. A total of 10,000,000 cells were implanted subcutaneously into the right flank of intact mice with Matrigel (#354234, Corning, BD Biocoat). For LAPC4-AR^{H875Y} xenograft assay, mice were castrated and randomly assigned into different groups when the xenografts reached approximately 150 mm^3 (length × width × width × 0.52). Water containing 5% sucrose and 2 mg/ml doxycycline was replaced every 2 days. The 90-day sustained-released progesterone pellets (15 mg, EZBioscience, China) were implanted subcutaneously for progesterone treatment. Each group consisted of 10 mice. For the GATA2 inhibitor assay, mice were castrated and randomly assigned into different groups when the xenografts reached approximately 250 mm^3 (length × width × width × 0.52). Mice were treated with K7174 (25 mg/kg, 2% DMSO + 98% 0.9% NaCl) daily, and xenografts were measured every other day with a caliper. Each group consisted of 10 mice. For the 3βHSD1 inhibitor assay, mice were castrated and randomly assigned into different groups when the xenografts reached approximately 150 mm^3 (length × width × width × 0.52). The 90-day sustained-released pregnenolone pellets (15 mg, EZBioscience, China) were implanted subcutaneously for pregnenolone treatment. Mice were treated with BCA (50 mg/kg, 5% DMSO + 95% corn oil) every day. Each group had 8 mice. Xenografts were measured every other day with a caliper. Student's t test was used for significance calculation. *, $P < 0.05$; **, $P < 0.01$.

BCA probe pull-down assay

Neutravidin resin (Thermo) was pre-incubated with GST at 4°C for 12 h before incubated with 50 μM biotin or BCA-biotin probe at 4°C. Purified GST-3βHSD1 protein as pre-incubated with DHEA (500 μM) or BCA (500 μM) before the addition of 25 μL packed BCA-biotin beads. Reactions were incubated for 4 h at 4°C for affinity capture. The binding beads were washed and eluted with loading buffer for immunoblotting detection.

CETSA

The assay was modified from a previously reported protocol. Cells were incubated with 20 μM DHEA (Steraloids Inc., USA), biochanin-A (MedChemExpress, Shanghai), or ethanol for 1 h in a CO_2 incubator. Cell pellets were resuspended with sucrose buffer (880 mM sucrose, 1.5 mM $CaCl_2$ in PBS), and centrifuged at 700 g for 30 min at 4°C. The supernatant was distributed and heated at different temperature endpoints (50-80°C) for 3 min in the Veriti 96-well thermal cycler. The supernatant was then centrifuged at 20,000 g for 20 min at 4°C and the soluble protein fraction in the supernatant was detected by western blot. Experiments were repeated at least three times independently.

Computational biochemistry

A homology model of human 3βHSD1 was built, as described in a previous report, based on the crystal structures of two related enzymes: the ternary complex of *E.coli* UDP-galactose 4-epimerase (UDPGE) with an NAD+ cofactor and substrate (PDB ID: 1NAH) and residues 154-254 of the ternary complex of human 17β-hydroxysteroid dehydrogenase (17βHSD1) with NADP and androstenedione (PDB ID: 1QYX) by Prime (Schrodinger, NY).[37] Protein minimization was then carried out by Prime. Virtual screening was performed based on this model and small molecule library from chemical biology core facility of SIBCB was used. For docking experiment, compounds were prepared and docked into the model at the SP precision by Induced Fit Docking (IFD) with NAD in the binding site. Compounds with the best docking score and IFD score were identified. The docked ligand-protein complexes in 3D were presented by PyMOL. Atoms of compound and NAD were represented as balls and sticks with carbon atoms in green and yellow, respectively, hydrogen atoms in white, oxygen atoms in red, nitrogen atoms in blue, phosphor atoms in orange. The whole protein is shown as cartoon, while the amino acids of the binding site are presented as lines, and those interacting with compounds are shown as sticks. Dashed lines represent hydrogen-bonds.

QUANTIFICATION AND STATISTICAL ANALYSIS

RNA-seq

Total RNA from each sample was extracted using the TRIzol reagent (Invitrogen, Waltham, MA, USA). VAHTS^{TM} mRNA-seq V3 Library Prep Kit for Illumina (NR611) was used for library construction, following the manufacturer's instructions. Briefly, 1000 ng of total RNA was used for the purification and fragmentation of mRNA. Purified mRNA was subjected to first- and second-strand cDNA synthesis. cDNA was then ligated to sequencing adapters (VAHTS^{TM} RNA Adapters set3 - set6 for Illumina, N809/N810/N811/N812) and amplified by PCR (using 12 cycles). The final libraries were evaluated using a Qubit Fluorometer (Invitrogen, USA) and QIAxcel Advanced System (QIAGEN, Valencia, CA, USA). Next, sequencing was performed on NovaSeq 6000 (PE150; Illumina, San Diego, CA, USA) by BerryGenomics Co., Ltd. (Beijing, China). The quality control of raw sequence data was evaluated by FastQC (v. 0.11.7), and the quality trimming and adapter clipping were performed using Trimmomatic (v.0.36-5). Paired-end reads were aligned to the GRCh38.91 human reference genome using hisat2 (v.2-2.1.0). Gene expression levels were quantified by HTSeq (v.0.11.1). The normalization of counts was performed using DESeq2 (v.1.24.0). Differential expression analyses were performed using DESeq2 based on the gene read count data. Biological triplicates were used in each treatment.

Pathway enrichment and gene set enrichment analysis

For pathway enrichment analysis, the differentially expressed genes were prepared for pathway enrichment with the MSigDB Investigate Gene Set module using hallmark gene sets (h.all.v7.2.symbols.gmt). For the gene set enrichment analysis, normalized counts were prepared for analysis using the GSEA 3.0. The hallmark gene sets (h.all.v7.2.symbols.gmt) were used and the genes were ranked as "Ratio_of_Classes" or "Signal2Noise". The permutation type selected was "gene_set" and other sets followed the default set of GSEA. The thresholds for inclusion were p <0.05 and q <0.25. The GSEA plot, normalized enrichment score, and the false discovery rate (FDR) q values were derived from GSEA output.

Statistics

Student's t-test, Fisher's exact test, and Log-rank test were performed to compare the differences between two groups. Pearson's correlation coefficient was used for the correlation analysis. * and ** denote $P < 0.05$ and $P < 0.01$, respectively. All analyses were performed using the GraphPad Prism 8.0 software. Data represent the mean ± standard deviation (SD), unless indicated otherwise.